

***Final Report: Immersion Tests to
Evaluate Corrosion of Alloy 22 in
Heated Brine Solutions***

Fuel Cycle Research & Development

***Prepared for
U.S. Department of Energy
Used Fuel Disposition
David Enos and Charles Bryan
Sandia National Laboratories
July 13th, 2012
FCRD-UFD-2012-000181
SAND 2012-5726***



DISCLAIMER

This information was prepared as an account of work sponsored by an agency of the U.S. Government. Neither the U.S. Government nor any agency thereof, nor any of their employees, makes any warranty, expressed or implied, or assumes any legal liability or responsibility for the accuracy, completeness, or usefulness, of any information, apparatus, product, or process disclosed, or represents that its use would not infringe privately owned rights. References herein to any specific commercial product, process, or service by trade name, trade mark, manufacturer, or otherwise, does not necessarily constitute or imply its endorsement, recommendation, or favoring by the U.S. Government or any agency thereof. The views and opinions of authors expressed herein do not necessarily state or reflect those of the U.S. Government or any agency thereof.

Sandia National Laboratories is a multi-program laboratory managed and operated by Sandia Corporation, a wholly owned subsidiary of Lockheed Martin Corporation, for the U.S. Department of Energy's National Nuclear Security Administration under contract DE-AC04-94AL85000.



Appendix E FCT Document Cover Sheet

Name/Title of Deliverable/Milestone: Final report: Immersion tests to evaluate corrosion of Alloy 22 in heated brine solutions
 Work Package Title and Number: Engineered Materials Performance - FT-12SN080506
 Work Package WBS Number: 1.02.08.03 Milestone Number: M3FT-12SN0805063
 Responsible Work Package Manager: Charles R. Bryan (Date Submitted): 7/13/12
 (Name/Signature)

Quality Rigor Level for Deliverable/Milestone	<input checked="" type="checkbox"/> QRL-3	<input type="checkbox"/> QRL-2	<input type="checkbox"/> QRL-1 <input type="checkbox"/> Nuclear Data	<input type="checkbox"/> N/A*
---	---	--------------------------------	---	-------------------------------

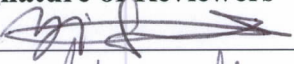
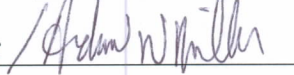
This deliverable was prepared in accordance with Sandia National Laboratories
(Participant/National Laboratory Name)

QA program which meets the requirements of
 DOE Order 414.1 NQA-1-2000 Other: FCT QAPD

This Deliverable was subjected to:

<input checked="" type="checkbox"/> Technical Review Technical Review (TR) Review Documentation Provided <input type="checkbox"/> Signed TR Report, or TR Report No.: _____ <input type="checkbox"/> Signed TR Concurrence Sheet (attached), or <input checked="" type="checkbox"/> Signature of TR Reviewer(s) below	<input type="checkbox"/> Peer Review Peer Review (PR) Review Documentation Provided <input type="checkbox"/> Signed PR Report, or PR Report No.: _____ <input type="checkbox"/> Signed PR Concurrence Sheet (attached), or <input type="checkbox"/> Signature of PR Reviewers below
---	---

Name and Signature of Reviewers

Yifeng Wang  Andrew Miller 	<u>7/12/12</u> <u>7-12-12</u>
(Name/Signature)	(Date)

*Note: In some cases there may be a milestone where an item is being fabricated, maintenance is being performed on a facility, or a document is being issued through a formal document control process where it specifically calls out a formal review of the document. In these cases, documentation (e.g., inspection report, maintenance request, work planning package documentation, or the documented review of the issued document through the document control process) of the completion of the activity along with the Document Cover Sheet is sufficient to demonstrate achieving the milestone. QRL for such milestones may also be marked N/A in the work package provided the work package clearly specifies the requirement to use the Document Cover Sheet and provide supporting documentation.

Page Intentionally Left Blank

SUMMARY

Corrosion experiments performed in the long term corrosion test facility (LTCTF) at Lawrence Livermore National Laboratory (LLNL) for the Yucca Mountain Project (YMP) were used to determine both the general corrosion rate and the temperature dependence of the general corrosion rate of Alloy 22 when exposed to repository relevant brines - data that were used in performance assessment calculations for the Yucca Mountain site. However, errors in sample preparation, contamination of the experimental systems with organic materials, and other experimental issues (SNL, 2010) have been identified that raise concerns regarding the corrosion data generated at the LTCTF. In an effort to verify the results of that experimental program, a series of exposure tests were initiated in late FY10. In these tests, Alloy 22 samples were prepared and then placed in solutions identified in the YMP model report *General and Localized Corrosion of the Waste Package Outer Barrier* (SNL, 2007). These solutions included 0.6M NaCl, simulated acidified water (SAW), and simulated concentrated water (SCW).

Under conditions where Alloy 22 is anticipated to be passive based upon the Pourbaix diagram for Cr in chloride-bearing solutions, the corrosion rate was found to be vanishingly small (i.e., below the resolution of the weight loss technique as implemented in this study). However, under low pH conditions where Alloy 22 is anticipated to be active, or more specifically, where the chromium oxide passive film is not thermodynamically stable, the corrosion rate was appreciable. Furthermore, under such conditions the corrosion rate was observed to be a strong function of temperature, with an activation energy of 72.9 ± 1.8 kJ/mol.

In the literature, it has been argued that sulfur may accumulate at the metal/oxide interface with time (Marcus, 2000). This sulfur originates from within the alloy, and builds in concentration as more of the metal is consumed by the corrosion reaction. It has been asserted that such accumulation of sulfur will eventually result in the depassivation of the material. While it has been clearly demonstrated by a number of researchers that the chromium and molybdenum present in engineering alloys such as Alloy 22 effectively mitigate any potential detrimental effects (Marcus, 2000 and 2002), this is not the case for nickel alloys that do not contain such additions. In the studies performed here, SAW samples evaluated at 60 and 90°C had an appreciable corrosion rate which, given the sulfur concentration within the material, may result in sulfur accumulation. Time of Flight-Secondary Ion Mass Spectroscopy (ToF-SIMS) analysis of the oxide layer revealed that while sulfur was present within the oxide for all conditions, no accumulation was observed at or near the metal/oxide interface.

Page Intentionally Left Blank

CONTENTS

SUMMARY	v
FIGURES	ix
TABLES	x
ACRONYMS	xi
1. Introduction	1
2. Experimental.....	1
2.1 Environments	1
2.2 Materials.....	2
2.3 Immersion Testing Procedures.....	3
2.4 Weight Loss Measurement Procedures.....	4
2.4.1 Coupon descaling.....	4
2.4.2 Mass Measurement	5
2.4.3 Uncertainty calculations.....	5
2.5 Solution Chemistry Measurement.....	6
3. Results	7
3.1 SAW.....	7
3.1.1 Weight Change as a Function of Temperature and Time.....	7
3.1.2 Thermal Activation Energy for General Corrosion in SAW.....	8
3.1.3 Surface Morphology as a Function of Temperature and Time	11
3.1.4 Oxide Chemistry as a Function of Temperature and Time	11
3.2 SCW.....	14
3.2.1 Weight Change as a Function of Temperature and Time.....	14
3.2.2 Analysis of Precipitates Formed In SCW.	15
3.2.3 Oxide Chemistry as a Function of Temperature and Time	20
3.3 0.5M NaCl.....	21
3.3.1 Weight Change as a Function of Temperature and Time.....	21
3.3.2 Surface Morphology as a Function of Temperature and Time	21
3.3.3 Oxide Chemistry as a Function of Temperature and Time	22
3.4 Evolution of Solution Chemistry	24
3.4.1 SAW.....	24
3.4.2 SCW.....	25
3.4.3 0.5M NaCl.....	26
3.4.4 Summary	28
4. Discussion.....	29
4.1 Thermal Activation Energy for General Corrosion of Alloy 22	29
4.2 General Corrosion Rate of Alloy 22 as a Function of Environment, Temperature, and Time.	29
5. Conclusions	31

6. References 31

Acknowledgements..... 31

Appendix 1: Mass Change Data..... 32

FIGURES

Figure 1: Pourbaix diagram for chromium in chloride-containing solutions (Pourbaix, 1974).....	2
Figure 2: Experimental configuration for long term corrosion performance testing, and PTFE sample racks used to suspend coupons within each container.....	4
Figure 3: Alloy 22 corrosion rate as a function of time in SAW at ambient temperature.	8
Figure 4: Alloy 22 corrosion rate as a function of time in SAW at 60°C.....	9
Figure 5: Alloy 22 corrosion rate as a function of time in SAW at 90°C.....	9
Figure 6: Alloy 22 corrosion rate as a function of temperature in SAW at 24 months.....	10
Figure 7: Activation energy calculation for samples exposed to SAW after 24 months. Based upon the data, the thermal activation energy was found to be 72.9 ± 1.8 kJ/mol. Error bars represent a single standard deviation and are shown for all three points.....	10
Figure 8: Surface morphology of coupons following 24 months of exposure in SAW at (a) ambient temperature, (b) 60°C, and (c) 90°C. Surface relief/contrast is due to the use of the Nomarski DIC imaging technique.....	11
Figure 9: Oxygen-18 signal as a function of depth for Alloy 22 coupons exposed to SAW at ambient, 60°C, and 90°C. The sharpness of the back edge of the oxygen peak indicates that the oxide is uniform or that the surface roughness is small, and as such, the thickness was taken as the depth at which the signal was 50% of the maximum level.....	12
Figure 10: Comparison of the oxygen-18 and sulfur profiles through the oxide and into the metal surface for samples exposed to SAW for a period of 24 months. Data is presented as the normalized intensity for each constituent. No evidence of sulfur accumulation was observed at the metal/oxide interface for any of the samples.....	13
Figure 11: Sample DWB071A exposed to SCW at 90°C for 24 months. Dark regions are bare metal, illustrating that the mirror polished surface was unaltered beneath the deposit.	14
Figure 12: XRD patterns for the 3-month and 24-month SCW test coupons. Upper—full pattern from 4° to 90° 2 θ . Lower—expanded view of the peaks below 40°.....	16
Figure 13: XRD patterns for the 3-month and 24-month SCW test coupons, along with matching phase patterns. The blue lines represent mordenite ($\text{Na}_{0.31}\text{Al}_{3.55}\text{Si}_{42.72}\text{O}_{96} \cdot 2.76\text{H}_2\text{O}$) (Pattern 01-080-0644); the green lines represent Ni-Cr-Co-Mo (Pattern 00-035-1489), which is iso-structural to Alloy 22. Upper—full pattern from 4° to 90° 2 θ . Lower—expanded view of the peaks below 40°.....	17
Figure 14: SEM Secondary electron image of zeolite coating on Alloy-22 coupon. The zeolite is well-crystallized, with orthorhombic crystals.....	18
Figure 15: EDS X-ray spectrum for the crystalline coating. The material is a Na, K, Al containing mordenite.	19
Figure 16: XRD pattern for precipitate from the SCW-90-1 reactor, along with matching phase patterns. The blue lines represent mordenite ($\text{Na}_{0.31}\text{Al}_{3.55}\text{Si}_{42.72}\text{O}_{96} \cdot 2.76\text{H}_2\text{O}$) (Pattern 01-080-0644); the red line represent magadiite ($\text{Na}_2\text{Si}_{14}\text{O}_{29} \cdot 10\text{H}_2\text{O}$) (Pattern 00-042-1350).....	19
Figure 17: Oxygen-18 signal as a function of depth for Alloy 22 coupons exposed to SCW at ambient and 60°C. The 90°C samples were not analyzed due to the extensive precipitate layer present. The sharpness of the back edge of the oxygen peak indicates	

that the oxide is uniform, and as such the thickness was taken as the depth at which the signal was 50% of the maximum level. 20

Figure 18: Comparison of the oxygen-18 and sulfur profiles through the oxide and into the metal surface for samples exposed to SCW for a period of 24 months. Data is presented as the normalized intensity for each constituent. No evidence of sulfur accumulation was observed at the metal/oxide interface for any of the samples. 21

Figure 19: Oxygen-18 signal as a function of depth for Alloy 22 coupons exposed to 0.5M NaCl at ambient, 60°C, and 90°C. The sharpness of the back edge of the oxygen peak indicates that the oxide is uniform, and as such the thickness was taken as the depth at which the signal was 50% of the maximum level. 22

Figure 20: Comparison of the oxygen-18 and sulfur profiles through the oxide and into the metal surface for samples exposed to 0.5M NaCl for a period of 24 months. Data is presented as the normalized intensity for each constituent. No evidence of sulfur accumulation was observed at the metal/oxide interface for any of the samples. 23

Figure 21: Corrosion Rate Distributions for 5 year Specimens in the LTCTF. 29

Figure 22: Corrosion rate as a function of temperature for the environments used to determine the temperature dependence of Alloy 22 in the LTCTF. 30

TABLES

Table 1: Solution Chemistries (M)..... 2

Table 2: Corrosion Rate vs. Time for Alloy 22 in SAW 7

Table 3: Oxide Thickness as a Function of Time in SAW 12

Table 4: Corrosion Rate vs. Time for Alloy 22 in SCW..... 14

Table 5: Oxide Thickness as a Function of Time in SCW..... 20

Table 6: Corrosion Rate vs. Time for Alloy 22 in 0.5M NaCl 21

Table 7: Oxide Thickness as a Function of Time in 0.5M NaCl 22

Table 8: Nominal and Measured SAW Test Solution Compositions (mg/L) 25

Table 9: Nominal and Measured SCW Test Solution Compositions (mg/L) 26

Table 10: Measured SCW 60°C, Bath 1 Test Solution Compositions (mg/L) Through Time. 26

Table 11: Nominal and Measured 0.5 M NaCl Test Solution Compositions (mg/L) 27

Table 12: Nominal and Measured 0.5 M NaCl Test Solution Compositions (mg/L) 27

Table 13: 24 Month Corrosion Rate as a Function of Environment 30

ACRONYMS

ACS	American Chemical Society
CR	Corrosion Rate
DI	Deionized
E _a	Activation Energy
EDS	Energy Dispersive Spectroscopy
IC	Ion Chromatography
ICP-OES	Inductively coupled plasma optical emission spectroscopy
LLNL	Lawrence Livermore National Laboratory
LTCTF	Long Term Corrosion Test Facility
NA	Not Analyzed
NIST	National Institute of Standards and Technology
nm	nanometer
PTFE	Polytetrafluoroethylene
QA	Quality Assurance
R	Gas constant
SA	Surface Area
SAW	Simulated Acidified Water
SCW	Simulated Concentrated Water
SD or σ	Standard Deviation
SNL	Sandia National Laboratories
T	Temperature
ToF-SIMS	Time-of-Flight Secondary Ion Mass Spectroscopy
ΔW	Weight change
XRD	X-ray Diffraction
YMP	Yucca Mountain Project

Page Intentionally Left Blank

Used Fuel Disposition Campaign

Final report: Immersion Tests to Evaluate Corrosion of Alloy 22 in Heated Brine Solutions

1. Introduction

Corrosion experiments performed in the long term corrosion test facility (LTCTF) at Lawrence Livermore National Laboratory (LLNL) for the Yucca Mountain Project (YMP) were used to determine both the general corrosion rate and the temperature dependence of the general corrosion rate of Alloy 22 when exposed to repository relevant brines, data that were used in performance assessment calculations for the Yucca Mountain site. However, errors in sample preparation, contamination of the experimental systems with organic materials, and other experimental issues (SNL, 2010) have been identified that raise concerns regarding the corrosion data generated at the LTCTF. In an effort to verify the results of that experimental program, a series of exposure tests were initiated in late FY10. In these tests, Alloy 22 samples were prepared and then placed in solutions identified in the YMP model report *General and Localized Corrosion of the Waste Package Outer Barrier* (SNL, 2007). These environments included 0.5M NaCl, simulated acidified water (SAW), and simulated concentrated water (SCW).

2. Experimental

The samples used to assess the general corrosion rate of Alloy 22 as a function of temperature were prepared and testing initiated under YMP technical work plan TWP-WIS-MD-000022 (SNL, 2008a). As will be discussed below, specimens were exposed to three different environments at three different temperatures (ambient, 60°C, and 90°C). Specimens were removed at a number of discrete time intervals and descaled, after which the total weight change associated with the sample was determined. The corrosion rate was then calculated based upon the total mass loss per unit area, per unit time.

2.1 Environments

In order to be consistent with the experiments performed at the LTCTF, the environments considered were dictated by the solutions used in that study. As such, SAW and SCW were selected. In addition, 0.5M NaCl was also explored, as it is a commonly evaluated test solution for marine applications. As defined in *General and Localized Corrosion of the Waste Package Outer Barrier* (SNL, 2010), the SCW test solution is three orders of magnitude (1,000×) more concentrated than J-13 well water and is slightly alkaline (pH approximately 10). The SAW test solution is also three orders of magnitude (1,000×) more concentrated than J-13 well water and is acidic (pH approximately 2.7). The target compositions of the three solutions are listed in Table 1 below.

The environments were selected based upon their anticipated impact on Alloy 22 as observed in prior testing performed in the LTCTF. In prior testing, SCW was found to be the most aggressive, followed by SAW. These results were somewhat counterintuitive based upon a conventional understanding of the corrosion performance of Ni-Cr-Mo alloys. Similar to stainless steels, Alloy 22 and other Ni-Cr-X based alloys rely on the formation of a protective chromium oxide layer which forms on the metal surface. It is the durability of this passive film which dictates the general and localized corrosion behavior of such materials. In the LTCTF study, while the SCW solution was found to be the most aggressive towards Alloy 22, that result was not consistent with what was anticipated based upon the Pourbaix diagram for an alloy which relies on chromium for the formation of the passive film (see Figure 1) (Pourbaix, 1974). Based upon the Pourbaix diagram, at the pH associated with SCW, the material should be passive and the corrosion rate very low. However, for SAW, where the pH is acidic, the material should not be passive, and should instead undergo general corrosion at a rate consistent with the material composition. Finally,

for the NaCl solution, with a pH near neutral, Alloy 22 should also be passive, with an extremely small corrosion rate.

Table 1: Solution Chemistries (M)

	0.5M NaCl	SAW	SCW
KCl	--	0.0950	0.0890
MgSO ₄	--	0.0022	--
NaF	--	0.0141	0.0660
NaNO ₃	--	0.3830	0.1090
Na ₂ SiO ₃	--	0.0007	0.0007
CaCl ₂	--	0.0020	--
NaHCO ₃	--	--	0.6000
Na ₂ SO ₄	--	0.4510	0.2000
NaCl	0.5000	0.5250	0.1000
NaOH	--	--	0.5000
pH	~ 7 (unadjusted)	2.7*	9.8 to 10.2*

* pH adjusted to target value with NaOH/HCl

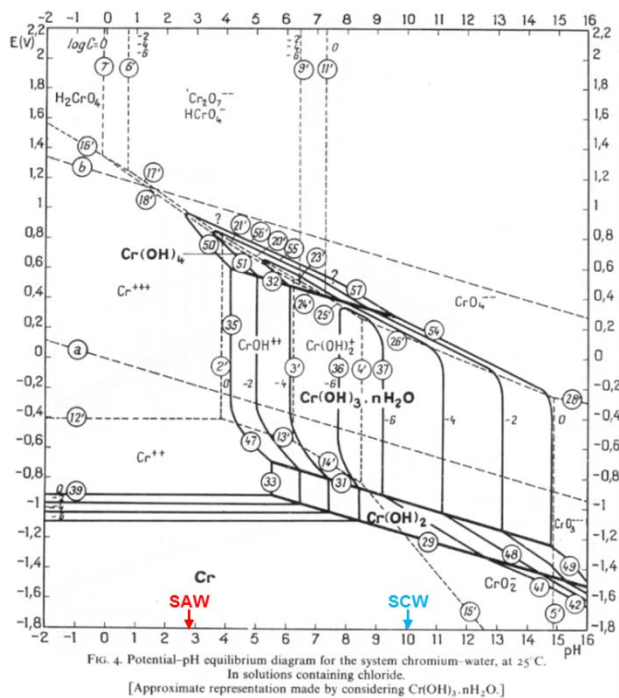


Figure 1: Pourbaix diagram for chromium in chloride-containing solutions (Pourbaix, 1974).

2.2 Materials

The material evaluated in this study was Hastelloy Alloy C22 (UNS N06022). This material is a Ni-Cr-Mo-W superalloy known to be highly corrosion resistant in oxidizing environments. In order to ensure the material was as close as possible to that evaluated in the LTCTF, coupons taken from that study were re-used for this one. Specimens used for the 6 month, 1 year, and 2 year sample time intervals in the LTCTF were re-polished for this study. In all cases, the original specimen identification was maintained, with the addition of an “A”, or if the sample was subdivided, with a “-1” or “-2” for each half

of the original coupon. By utilizing the same material as was used in the LTCTF, any variation in performance due to compositional differences has been removed.

The front and rear surface of each coupon was polished to a mirror finish via conventional metallographic techniques, while the edges were mechanically ground to a 600 grit finish. Once polished, each sample was chemically cleaned. The cleaning/passivating procedure included first degreasing in acetone, followed by a three minute soak in 15 vol% HCl. For each treatment, a single coupon was canted horizontally in a 250 mL beaker containing 200 mL of stirring acetone or HCl solution. All solutions were kept at ambient temperature. The samples were individually degreased in acetone for three minutes to remove residual machining residue, after which they were briefly submersed in deionized (DI) H₂O and blown dry using filtered, dry nitrogen. The coupons were placed in a 105 °F forced air dryer for 15 minutes to complete the drying process, and were allowed to cool before any subsequent handling. While the acetone was replenished as necessary during the degreasing process, each 200 mL 15 vol% HCl sample was used for no more than five individual coupons due to the concern of increasing aggressiveness of the solution due to metal ion buildup. After each coupon was soaked in 15 vol% HCl for 3 minutes, the sample was immediately rinsed in a larger volume (300-400 mL) of DI H₂O. The coupon was removed and immediately placed under flowing DI H₂O for two minutes. It was then blown dry using filtered, dry nitrogen and placed in a 105 °F forced air dryer for 15 minutes.

Once cooled, the initial weight of each coupon was documented. The coupon length, width, and thickness dimensions were recorded using calibrated Fowler Sylvac calipers, and the samples surface area calculated.

2.3 Immersion Testing Procedures

In these tests, Alloy 22 samples were prepared and then placed in solutions identified in the Yucca Mountain model report *General and Localized Corrosion of the Waste Package Outer Barrier* (SNL, 2007). These environments included 0.5M NaCl, SAW, and SCW. Care was taken to insure each sample had a nominally identical surface finish, and had been chemically cleaned/passivated in the same manner prior to exposure.

For elevated temperature exposures, the exposure tanks (see Figure 2) consisted of 5 liter, round bottom glass flasks that are O-ring flanged at the top opening. There were two flasks for each environment/temperature combination, for a total of 12 temperature controlled tanks. Each flask employs a glass cover with five ground glass joints accommodating an Allihn drip tip glass condenser, PFA fluoropolymer coated control thermocouple, aeration plumbing and access ports. Each bath is heated with a Electrothermal 800 watt mantle heater controlled by two Omega model C111517-TC-2 process controllers running Omega model URM-800 relay modules with twelve Omega CASS-18G-18-PFA input thermocouples. Bath condensers are chilled in multiples of two (one 60°C bath and one 90°C bath) with six VWR / Polyscience model 1166 refrigerated liquid circulators. Ambient temperature baths consisted of three rectangular glass ten gallon tanks having domed polycarbonate covers and three access holes for temperature measurement, aeration and fill. Bath aeration is accomplished with a Barnant model 400-1901 air pump supplying a tube manifold with twelve Swagelok "S" series metering valves for each bath.

Specimens were placed on polytetrafluoroethylene (PTFE) rods, and hung on a PTFE rack as illustrated in Figure 2. Three groups of four coupons (1 complete rack) were placed in each of the elevated temperature baths. As the ambient temperature containers were larger, each one held two racks. Each rack held three sets of four samples. Sample to sample contact was prevented by PTFE spacers between adjacent samples on the rod which the samples were held. This arrangement allowed a single group of specimens to be removed at each time interval. Two complete racks were evaluated in each environment, with a total of 8 coupons being removed from each environment at each test interval. One of the coupons was for surface analysis, while the remaining 7 were used to evaluate the corrosion rate.

The test program itself was initiated prior to the shutdown of the YMP under Yucca Mountain quality assurance (QA) procedures. The governing QA document is Technical Work Plan: *General and Localized Corrosion Testing of Waste Package and Drip Shield Materials* (SNL, 2008a), and testing has been consistent with the procedures described in that document, with the exception of planned sampling times. As a result of the shutdown, funding was not available to remove samples at the prescribed time periods, and new time intervals have been chosen. Specimens were removed after 3, 9, 18, and 24 months of exposure. Samples of each solution were taken when coupons were removed, and stored for later compositional analysis. The 3 month exposure was performed after the 18 month coupons were removed from the baths. (i.e., new samples were added to the middle level on the sample racks after the 18 month coupons were removed)

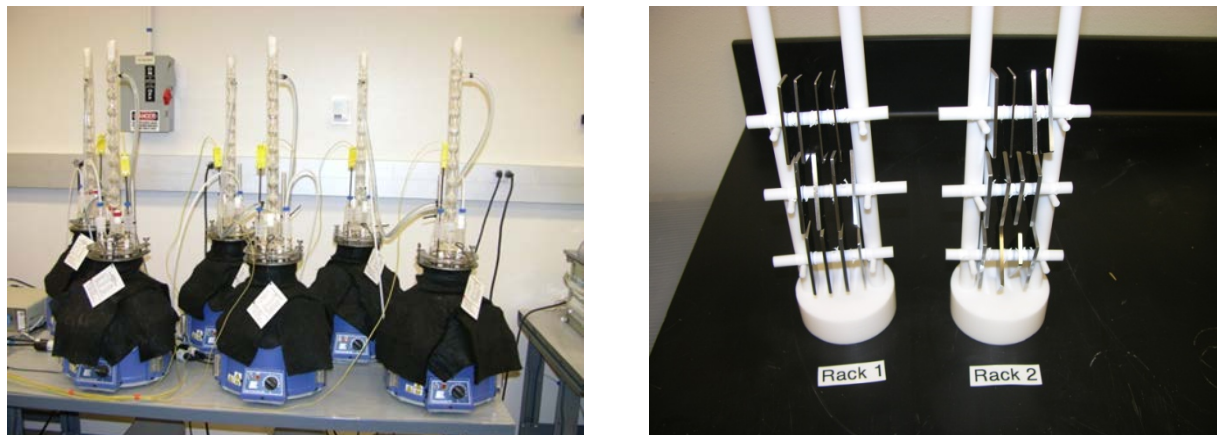


Figure 2: Experimental configuration for long term corrosion performance testing, and PTFE sample racks used to suspend coupons within each container.

2.4 Weight Loss Measurement Procedures

2.4.1 Coupon descaling

When samples were removed from baths, care was taken to minimize drying of the test solutions on the surfaces of samples. The removed samples were placed immediately in DI H₂O to prevent drying of the bath solution on the coupon surface. Each coupon was rinsed for 2 minutes in flowing DI H₂O, blown dry using filtered, dry nitrogen, and then placed in a 105 °F forced-air dryer for 15 minutes. The coupons were stored in a nitrogen cabinet throughout the entire descaling process.

All coupons underwent three cycles of descaling following a procedure based upon TST-PRO-T-008 (SNL, 2008c) using 15 vol% HCl to remove any corrosion product or residual bath deposits present on the coupon surface. Between each descaling sequence, the weight of each coupon was recorded per the mass measurement procedure. The first coupon weight was recorded after the coupons were removed from the baths and rinsed; this weight was termed the coupon “as removed” weight. The coupons were descaled using 15 vol% HCl and then reweighed. The descaling and weighing cycle was repeated no less than three times until the coupon weight was stable to 10 µg between descaling cycles.

The coupon descaling procedure used is similar to that described in the sample preparation section (Section 2.3). The first descaling was preceded by a three minute acetone soak to remove any organic material which might have been deposited on the surface. Each coupon was canted horizontally in a stirred 200 mL sample of acetone contained in a 250 mL beaker for a total of 3 minutes. The coupon was immediately submerged in DI H₂O after removal from the acetone beaker, after which it was blown dry using filtered, dry nitrogen. The coupon was then placed in a 105 °F dryer for no less than 15 minutes,

and allowed to cool completely. Next, coupons were descaled in 15 vol% HCl for 3 minutes. Again, individual sample coupons were canted horizontally in a 200 mL sample of stirring HCl contained in a 250 mL beaker. After 3 minutes, each coupon was immediately rinsed in a stagnant beaker containing DI H₂O (300-400 mL) as a pre-rinse, and then immediately (i.e., specimens did not dry between steps) rinsed under flowing DI H₂O for two minutes. The coupon was blown dry using filtered, dry nitrogen and then placed in a 105 °F dryer for no less than 15 minutes. All subsequent descaling cycles included only a 3 minute HCl soak; the acetone step was used only preceding the first HCl descaling. Samples of HCl were replaced after cleaning/descaling 5 coupons to prevent exposure of the coupons to a more aggressive acidic environment from metal ion dissolution. The DI H₂O pre-rinse bath was also replaced after 5 uses.

2.4.2 Mass Measurement

The weight measurements were performed following a modified National Institute of Standards and Technology (NIST) single substitution technique, as defined in TST-PRO-T-006 (SNL, 2008b). A high precision analytical balance (Mettler XP105DR), combined with a weight set calibrated by the Primary Standards Laboratory at SNL to the highest level of precision they could accomplish was used for all measurements. Care was taken to ensure that the balance was always at operating temperature prior to making any measurements. This was accomplished by leaving the balance turned on continually throughout the entire measurement duration.

Prior to performing each set of measurements, the balance was zeroed and its self-calibration routine was executed. The laboratory temperature, pressure, and relative humidity were recorded at the beginning and end of each sample collection period. At the beginning and upon completion of each measurement cycle, the sample coupon weight measurements were bounded in time with calibrated weigh standard measurements to monitor and account for balance drift. The mass standards were weighed at the beginning and end of each data set collection. They were also weighed after recording the weights of every 6 coupons. If a pause in weighing the sample coupons was taken, the standards were weighed before stopping collecting weight measurements and again before restarting measurement collection. Mass standards of 20, 5, and 2 grams were used to obtain total standard weights of 20, 25, and 27 grams. The set of three standard weights was chosen to account for balance linearity among coupons with a similar weight range. Each standard and coupon was weighed three times, and the average weight was used for all calculations. If the balance zero drifted at any point, it was reset to zero.

2.4.3 Uncertainty calculations

Both balance drift and measurement uncertainties were calculated for each coupon weight following the general guidelines in TST-PRO-T-006 (SNL, 2008b). Each weight measurement was adjusted for balance drift using the difference between a measured standard's true weight and its apparent measured weight. The standard closest to the coupon weight was used: a coupon with a weight around 24g would require use of the 25g standard weight value to compensate for balance drift. The true standard weight was obtained from standard calibration. Standard weights measured before and after the coupon weight were both used. Once the difference between each of these two standards and the true standard mass was calculated, the average standard difference was used to adjust the coupon weight value.

The uncertainty in the measurement of each coupon was also calculated. Both the coupon weight measurement and the standard weight measurement contribute to the coupon measurement uncertainty. The coupon weight measurement uncertainty used is the standard deviation (1σ) of the measurements recorded. The uncertainty in the standard weight was obtained from calibration. A sum of squares combination of these two uncertainties was used to obtain the final coupon measurement uncertainty. For the calculated total coupon weight loss, a sum of squares combination of the initial coupon weight and the final coupon weight yielded the total weight loss uncertainty.

2.5 Solution Chemistry Measurement

Inductively coupled plasma optical emission spectrometry (ICP-OES) was used to measure solution concentrations of the cations Na, K, Mg, Ca, Si, and Al; S was also measured and used to calculate sulfate concentrations. Chloride, fluoride, and nitrate were measured by ion chromatography (IC). The results of the SAW, SCW, and 0.5 M NaCl brines analyses are presented in the following discussion. The nominal concentrations of the major elements in the prepared solutions, as calculated from the brine formulas (Table 1) are provided for comparison. It should be noted that the reported nominal Na and Cl values do not account for use of NaOH and HCl to adjust the pH of the test solutions in the final step of preparation; the measured concentrations Na, Cl, or both in SAW and SCW are expected to deviate from the nominal values for this reason. Also provided are charge balance errors for the SAW and 0.5 M NaCl brines. Although carbonate/bicarbonate concentrations were not measured, these phases would contribute negligibly to the ionic strength of those two brines, and charge balances provide a metric for evaluating the quality of the analyses. Charge balances are calculated using:

$$\text{Charge balance error, \%} = \frac{(\text{Equiv}_{\text{cations}} - \text{Equiv}_{\text{anions}})}{(\text{Equiv}_{\text{cations}} + \text{Equiv}_{\text{anions}})} \times 100$$

The charge balance is positive if the analysis has excess cations (that is, if the sum of the equivalents of the cations is greater than the sum of the equivalents of the anions), and negative if the analysis has excess anions.

3. Results

3.1 SAW

3.1.1 Weight Change as a Function of Temperature and Time

The corrosion rate was calculated from the weight change data as:

$$CR = \frac{\Delta W}{\rho \times SA \times t}$$

Where ΔW is the total measured weight change (i.e., initial weight – post-descaling weight), ρ is the density of Alloy 22 (8.69 g/cm³), SA is the surface area of the test coupon, and t is the total exposure time. The average results are presented in Table 2. At ambient temperature, the corrosion rate was unresolvable using the weight-loss method as implemented in this study. As the temperature increased to 60°C, a readily resolvable corrosion rate was observed. This rate was larger at 3 months, then decreased and remained fairly constant for times beyond that point. The elevated corrosion rate at short times is consistent with the behavior of other corrosion resistant materials. Furthermore, the constant corrosion rate with time, even at 24 months, indicates that this is a general corrosion process, as anticipated from the Pourbaix diagram. The same basic behavior was observed at 90°C, albeit with a corrosion rate nearly an order of magnitude larger.

It should be noted that in some cases, the magnitude of the weight change observed is on the order of the resolution of the weight-loss technique as implemented in this study. As a result, there were cases where the weight change was slightly negative, and as a result, the calculated corrosion rate is slightly negative. In such cases, while the calculated “corrosion rate” is negative, the actual rate is effectively zero.

Table 2: Corrosion Rate vs. Time for Alloy 22 in SAW

	Ambient		60°C		90°C	
	CR (nm/yr)	1 SD	CR (nm/yr)	1 SD	CR (nm/yr)	1 SD
3 months	-3.7	12.8	63.9	12.7	499.3	12.8
9 months	6.1	4.4	47.9	4.3	475.6	4.3
18 months	0.9	2.6	47.3	2.6	474.3	2.6
24 months	1.7	1.6	45.7	1.6	457.2	1.6

SD = standard deviation

The distribution of calculated corrosion rates at ambient temperature as a function of time is presented in Figure 3. The scatter in the data was large at 3 months, and then decreased in magnitude as time progressed. This behavior is the result of the formula used to determine the corrosion rate. Given that the accuracy of the weight change measurements themselves is on the order of 30 micrograms, as the time increases, that uncertainty in weight change represents an increasingly small uncertainty in the apparent corrosion rate. This is reflected in the calculated values presented in Table 2.

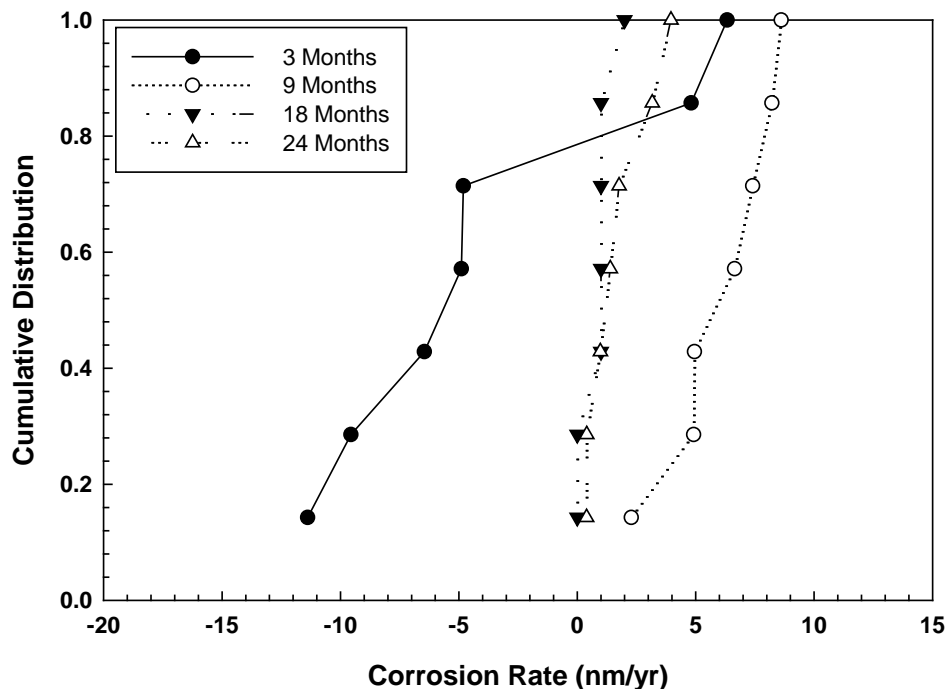


Figure 3: Alloy 22 corrosion rate as a function of time in SAW at ambient temperature.

The distribution of corrosion rates as a function of time at 60°C is presented in Figure 4. As with the ambient temperature samples, a wider distribution was observed at shorter exposure times than at longer times. At 3 months, there was a single outlier with a corrosion rate considerably larger than the others. While evaluating the sample after the cleaning process was complete, it was noticed that there were numerous scratches in the finish. Given that the difference in weight loss between the outlier and the remainder of the population was less than 200 micrograms, it is likely that the larger weight change can be explained by the scratches, rather than an increased dissolution rate relative to the other coupons. The distributions at 18 and 24 months were nominally identical, indicating that the process was stable.

The distribution of corrosion rates as a function of time at 90°C is presented in Figure 5. As with the other temperatures, the distribution narrowed with increasing time, indicating that the dissolution rate was stabilizing.

3.1.2 Thermal Activation Energy for General Corrosion in SAW

The distribution of corrosion rates as a function of temperature at 24 months is presented in Figure 6. In the previous long term corrosion experiments performed in the LTCTF, no environmental dependence was seen in the average general corrosion rate (counter to what was predicted based upon the Pourbaix diagram (Figure 1)), and furthermore, no temperature dependence of the general corrosion rate was observed when comparing data taken at 60°C and 90°C. This was inconsistent with the results obtained in this study. As illustrated in Figure 6, there is a clear temperature dependence of the general corrosion rate for Alloy 22 in SAW.

Furthermore, the data follows Arrhenius kinetics (i.e., $= A \exp\left(-\frac{E_a}{RT}\right)$, where A is a constant, E_a the activation energy, R the gas constant, and T the temperature), as illustrated in Figure 7. By plotting the log of the corrosion rate as a function of inverse temperature, a straight line is achieved. The slope of this line is proportional to the thermal activation energy. The calculated activation energy was found to be 72.9 ± 1.8 kJ/mol.

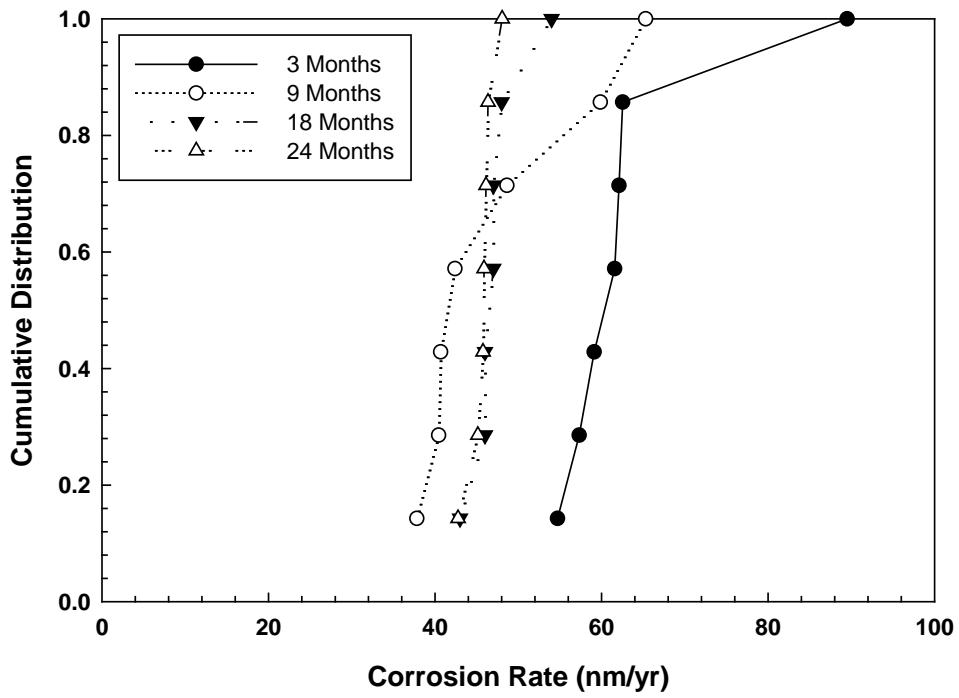


Figure 4: Alloy 22 corrosion rate as a function of time in SAW at 60°C.

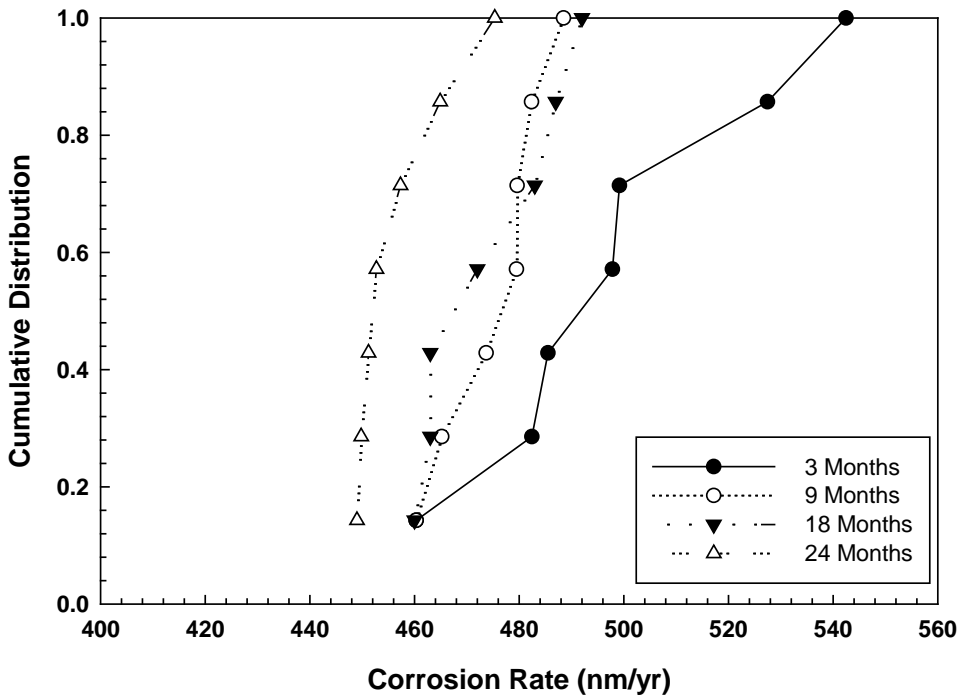


Figure 5: Alloy 22 corrosion rate as a function of time in SAW at 90°C.

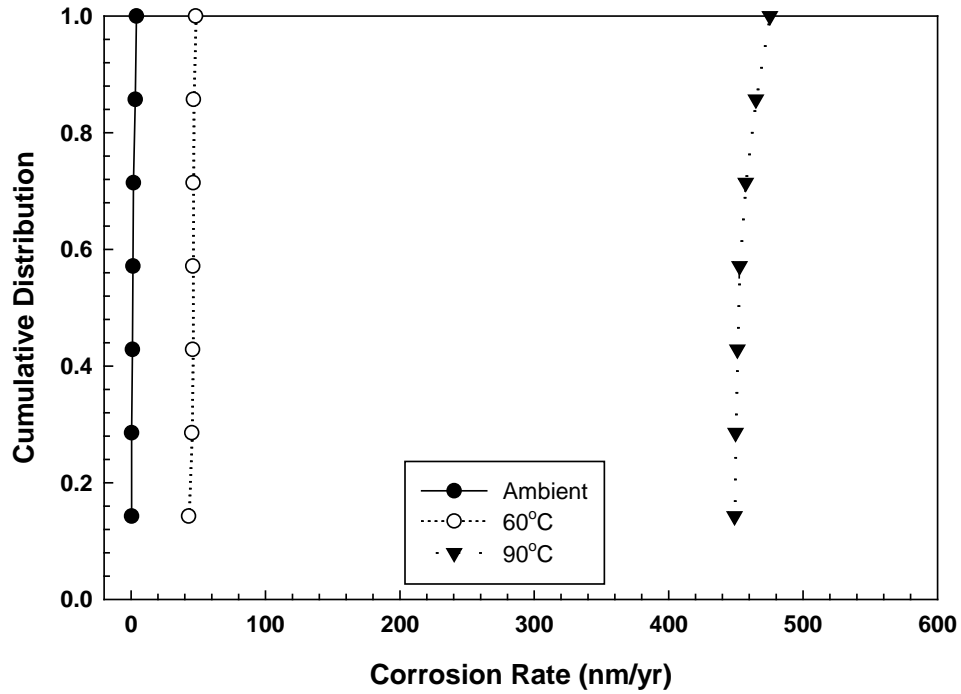


Figure 6: Alloy 22 corrosion rate as a function of temperature in SAW at 24 months.

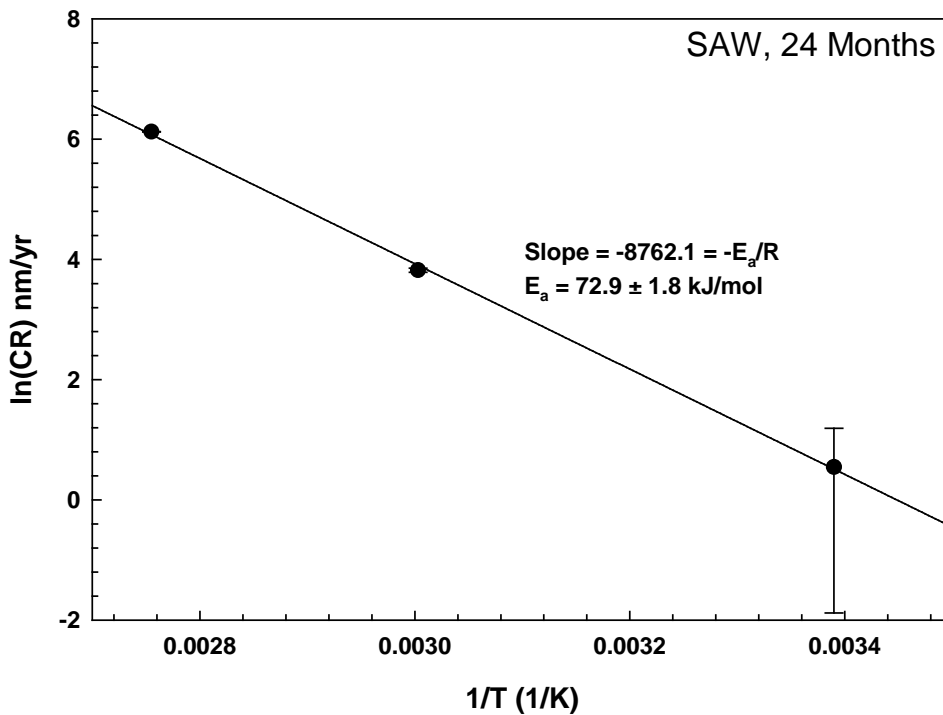


Figure 7: Activation energy calculation for samples exposed to SAW after 24 months. Based upon the data, the thermal activation energy was found to be 72.9 ± 1.8 kJ/mol. Error bars represent a single standard deviation and are shown for all three points.

3.1.3 Surface Morphology as a Function of Temperature and Time

In order to corroborate the weight change results, the surface of samples taken from each temperature were evaluated optically. In Figure 8 it can be seen that after 24 months exposure at ambient temperature, the polishing marks were still clearly visible on the surface, indicating that little, if any, dissolution had taken place. For the sample exposed to 60°C, the polishing marks were gone, and the surface had been smoothed. In addition, some relief on the surface was visible correlating with the underlying microstructure. This observation is consistent with the low, but readily measured, corrosion rate observed for these specimens. At 90°C, where the dissolution rate was an order of magnitude larger, the surface had been etched, revealing the underlying microstructure (grain boundaries, twins, etc.). As with the 60°C sample, the polishing marks are gone

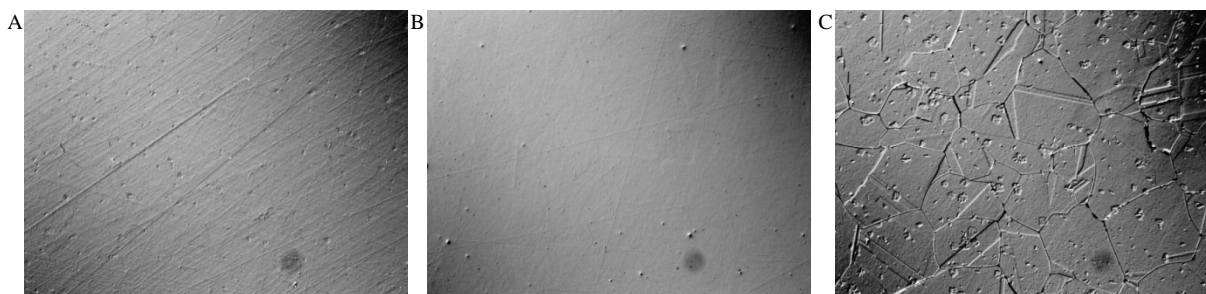


Figure 8: Surface morphology of coupons following 24 months of exposure in SAW at (a) ambient temperature, (b) 60°C, and (c) 90°C. Surface relief/contrast is due to the use of the Nomarski DIC imaging technique.

3.1.4 Oxide Chemistry as a Function of Temperature and Time

Time-of-Flight Secondary Ion Mass Spectroscopy (ToF-SIMS) was used to probe the composition of the oxide layer on the surface of the Alloy 22 coupons as a function of time. Upon the completion of each exposure test time interval, a single coupon from each test condition was set aside for surface analysis. Aside from rinsing in deionized water, no cleaning procedures were applied to these coupons. Due to the complexity of the oxide layer, and the lack of an appropriate set of standards, exact compositions could not be reported. While this data cannot be used to identify exact compositions, it can be used to determine the relative concentrations and locations of various constituents within the oxide. To evaluate the oxide thickness, the less abundant ^{18}O isotope was used, rather than the more abundant ^{16}O isotope because the ^{16}O signal tended to be too large, overwhelming the detector. The ^{18}O profiles for coupons exposed to SAW as a function of temperature and time are presented in Figure 9. Since the oxide layer was reasonably uniform, it was possible to determine the thickness of the oxide layer as the depth at which the signal dropped to half its maximum intensity. The oxide thicknesses determined in this manner are presented in Table 3. It should be noted that while 3 representative regions on each sample were analyzed, the results presented here are from a single analysis area, and as such do not capture the variability which no doubt exists both within a single coupon or when comparing similar coupons.

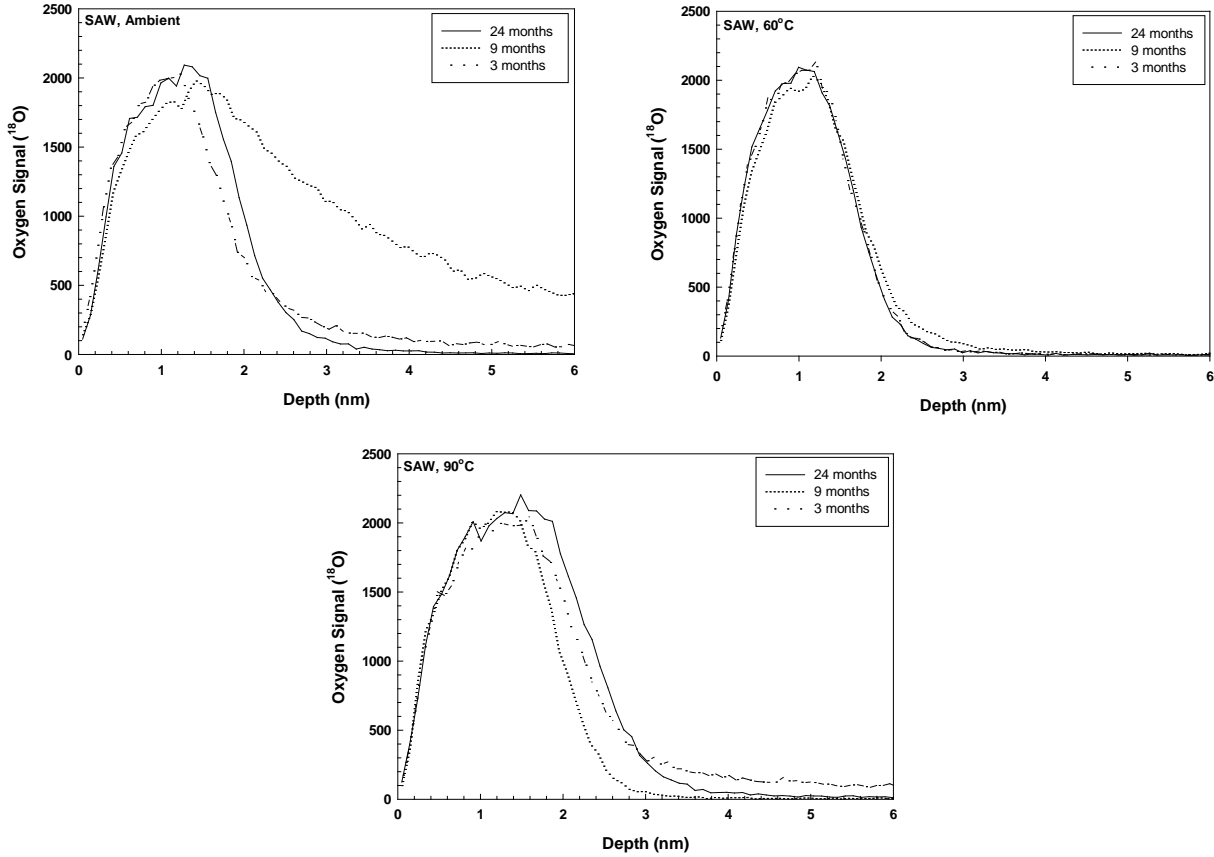


Figure 9: Oxygen-18 signal as a function of depth for Alloy 22 coupons exposed to SAW at ambient, 60°C, and 90°C. The sharpness of the back edge of the oxygen peak indicates that the oxide is uniform or that the surface roughness is small, and as such, the thickness was taken as the depth at which the signal was 50% of the maximum level.

Table 3: Oxide Thickness as a Function of Time in SAW

	Oxide Thickness (nm)		
	3 Months	9 Months	24 Months
Ambient	1.8	*	2
60°C	1.7	1.7	1.7
90°C	2.3	2	2.4

*The gradual slope of the back edge indicates that the surface was not uniform

In the literature, it has been argued that sulfur may accumulate at the metal/oxide interface with time (Marcus, 2000). This sulfur originates from within the alloy, and builds in concentration as more of the metal is consumed by the corrosion reaction. While it has been clearly demonstrated by a number of researchers that the chromium and molybdenum present in engineering alloys such as Alloy 22 effectively mitigate any potential detrimental effects (Marcus, 2000 and 2002), this is not the case for nickel alloys which do not contain such additions. In the studies performed here, SAW samples evaluated at 60 and 90°C had an appreciable corrosion rate which, given the sulfur concentration within the material, may result in sulfur accumulation. ToF-SIMS analysis of the oxide layer revealed that sulfur was present within the oxide for all conditions, including the ambient temperature exposure, suggesting that the

material in the oxide was the result of the constituents of the exposure solution. To better illustrate the location of sulfur in regions near the metal/oxide interface, the normalized intensity of oxygen and sulfur were compared for the 24 month samples, as shown in Figure 10. The absolute concentrations of oxygen and sulfur were not determined, but the relative amount of sulfur within the oxide can clearly be seen. The large peak near about 0.3 nm depth indicates sulfur on the surface of the oxide. In ambient conditions, where no measurable corrosion has taken place, sulfur is observed within the oxide layer, decreasing to effectively zero at the metal/oxide interface. The secondary peak observed in the oxide is also seen in other coupons which underwent minimal dissolution, as will be demonstrated later in the text for SCW and 0.5M NaCl. This observation suggests that sulfur is introduced into the oxide either through the sample preparation process, or from constituents of the exposure solution. A nearly identical result is seen at 60°C. For the 60°C samples, with an average corrosion rate of 45.7 ± 1.6 nm/yr, no additional sulfur was built up at or near the metal/oxide interface. At 90°C, the average corrosion rate was an order of magnitude larger at 457.2 ± 1.6 nm/yr, and as such, that much more sulfur would be available to accumulate at the metal/oxide interface. However, as with the lower temperatures, sulfur accumulation was not observed at the metal/oxide interface.

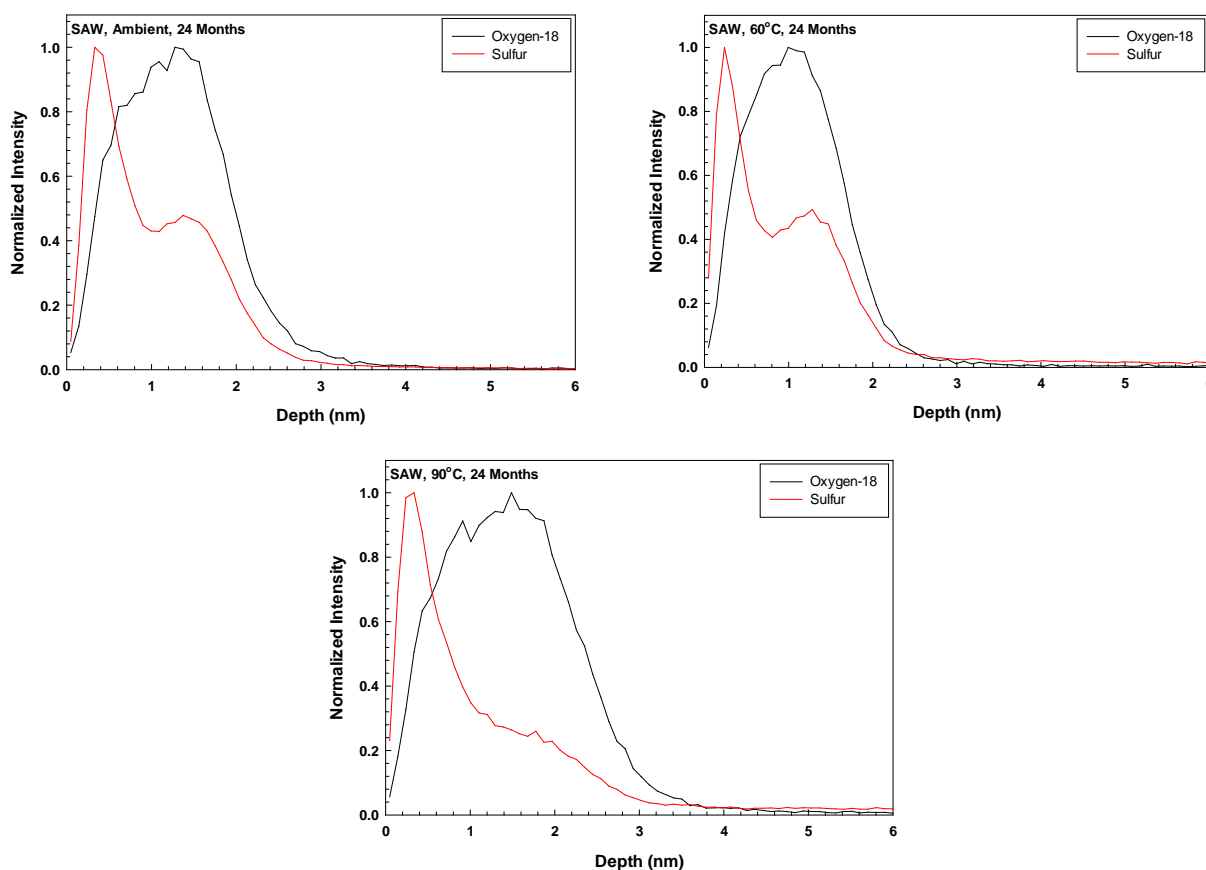


Figure 10: Comparison of the oxygen-18 and sulfur profiles through the oxide and into the metal surface for samples exposed to SAW for a period of 24 months. Data is presented as the normalized intensity for each constituent. No evidence of sulfur accumulation was observed at the metal/oxide interface for any of the samples.

3.2 SCW

3.2.1 Weight Change as a Function of Temperature and Time

As discussed above, based upon the Pourbaix diagram, it was anticipated that Alloy 22 should be electrochemically passive in SCW, and as such have an extremely small dissolution rate. The resulting corrosion rates, calculated in the same manner as described above for SAW, are presented in Table 4. In all cases, the corrosion rate was effectively below the ability of the weight loss technique to detect it. One complicating factor for this solution was the observation of considerable precipitation of solution components with time, particularly at 90°C, as illustrated in Figure 11. As discussed for SAW, in some cases the overall weight change was below our ability to effectively resolve it, and the measured value was slightly negative resulting in a negative apparent “corrosion rate”. The actual rate in such cases is effectively zero.

Table 4: Corrosion Rate vs. Time for Alloy 22 in SCW

	Ambient		60°C		90°C	
	CR (nm/yr)	1 SD	CR (nm/yr)	1 SD	CR (nm/yr)	1 SD
3 months	0.0	12.8	0.9	12.7	*NA	
9 months	9.7	4.5	4.4	4.3	-2.5	4.3
18 months	-0.6	2.6	-1.9	2.6	-3.0	2.6
24 months	0.3	1.6	-1.1	1.6	*NA	

*Surface deposits from the solution hindered analysis of the weight change



Figure 11: Sample DWB071A exposed to SCW at 90°C for 24 months. Dark regions are bare metal, illustrating that the mirror polished surface was unaltered beneath the deposit.

While the deposits on the sample surfaces were not particularly tenacious, the use of mechanical means to remove them was not possible due to the impact which any small scratches would have on the observed weight loss. As such they had to be chemically removed, which proved difficult. Two procedures were found to be effective in removing the deposits – soaking in a commercially available alkaline cleaner (10% Brulin 815GD) or soaking in a 1M NaOH solution. Unfortunately, both of these techniques tended to remove some of the underlying material, both on blank coupons as well as the test specimens themselves. Thus, while the final weight changes were on the order of 30 to 200 micrograms,

a similar result was observed for blank (unexposed) coupons. As such, though the results indicate a negligible degree of mass loss, the weight change data from these coupons could not be reliably used to calculate the overall general corrosion rate.

3.2.2 Analysis of Precipitates Formed In SCW.

At elevated temperatures, especially at 90°C, the SCW solutions became cloudy over time, and a large mass of precipitate formed. Moreover, coupons immersed in this solution at 60°C and 90°C for up to two years were coated with a white precipitate. Removal of the precipitate, required to evaluate corrosion rates through mass loss, was accomplished only with difficulty, and analysis of the coating was undertaken to aid in cleaning. Also, during post-test sampling of the brines used in the immersion tests, the voluminous precipitate in the bottom of the elevated-temperature SCW baths was sampled to determine its composition and source.

Analysis of the SCW brine composition using EQ3/6 version 8.0 and the Pitzer database developed for Yucca Mountain Project indicated that, within the limits of the database mineral list, which contains an exhaustive suite of evaporates, nothing was saturated or even close to saturation in the nominal brine composition. However, components may have been added to the brine from leaching or dissolution of two sources, the Alloy 22 coupons or the borosilicate glass exposure vessels. As Alloy 22 coupons that have been cleaned of precipitate show negligible weight loss (that is, no significant corrosion), it is unlikely that Alloy 22 components are contributing to the white coating on the coupons, or to the voluminous precipitate in the baths. The glass containers, therefore, were suspected of leaching silica and other species into the solution.

To identify the phase present, the coatings on two Alloy 22 test coupons was analyzed by X-ray diffraction (XRD). The two samples evaluated were SCW-90-1 3 months (ARC22-62-1), and SCW-90-1 24 months (DWB071A). The 3-month sample had a thin but continuous coating of the whitish precipitate, while the 24-month sample had a much thicker coating that had flaked off in places. The coatings were analyzed *in situ*, on the Alloy 22 coupons. The two patterns are shown in Figure 12. The patterns are very similar, with almost all peaks coinciding. Major features include three large peaks at 43°, 51°, and 74° and a suite of smaller peaks at 2θ angles of less than 50°. With one exception (at 10°) the peaks occurring below 50° have a greater intensity for the more-thickly coated 24-month sample than for the 3-month sample. They are interpreted to be representative of the mineral coating. Conversely, the three large peaks at >40° 2θ are more intense for the 3-month sample, and also correspond to smaller d-spacings; they are interpreted to represent the Alloy-22 substrate.

Both patterns, but especially that for the 24-month sample, show a strong asymmetry in the peaks at angles of lower than 20°; the lowest-angle peaks for the 24-month sample are actually doubled. These additional peaks are artifacts, and are probably due to secondary fluorescence of iron in the Alloy 22 substrate.

Two phases were identified in the patterns (Figure 13). As suspected, the three high intensity peaks at >40° 2θ represent the Alloy 22 substrate. Although Alloy 22 is not in the powder diffraction database, a suite of iso-structural (face-centered cubic) alloys are present, and these fit the observed peaks well. The matching pattern shown in Figure 13 is a Ni-Cr-Co-Mo alloy (Card # 00-035-1489), but several structurally-similar other compounds match the peaks well, including γ-(Fe,Ni) (Card # 00-047-1417); 304 stainless steel (Card # 00-033-0397); and Fe_{0.64}Ni_{0.36} (Card # 00-047-1405).

The XRD pattern of the precipitate matches that of the zeolite mineral mordenite. Compositionally, naturally occurring mordenite is (Ca, Na₂, K₂)Al₂Si₁₀O₂₄ • 7H₂O. Several variations of this are in the powder diffraction database; they vary little in terms of peak location, and all fit the observed pattern well. The pattern shown in Figure 13 is for a synthetic mordenite, Na_{0.31}Al_{3.55}Si_{42.72}O₉₆ • 2.76 H₂O.

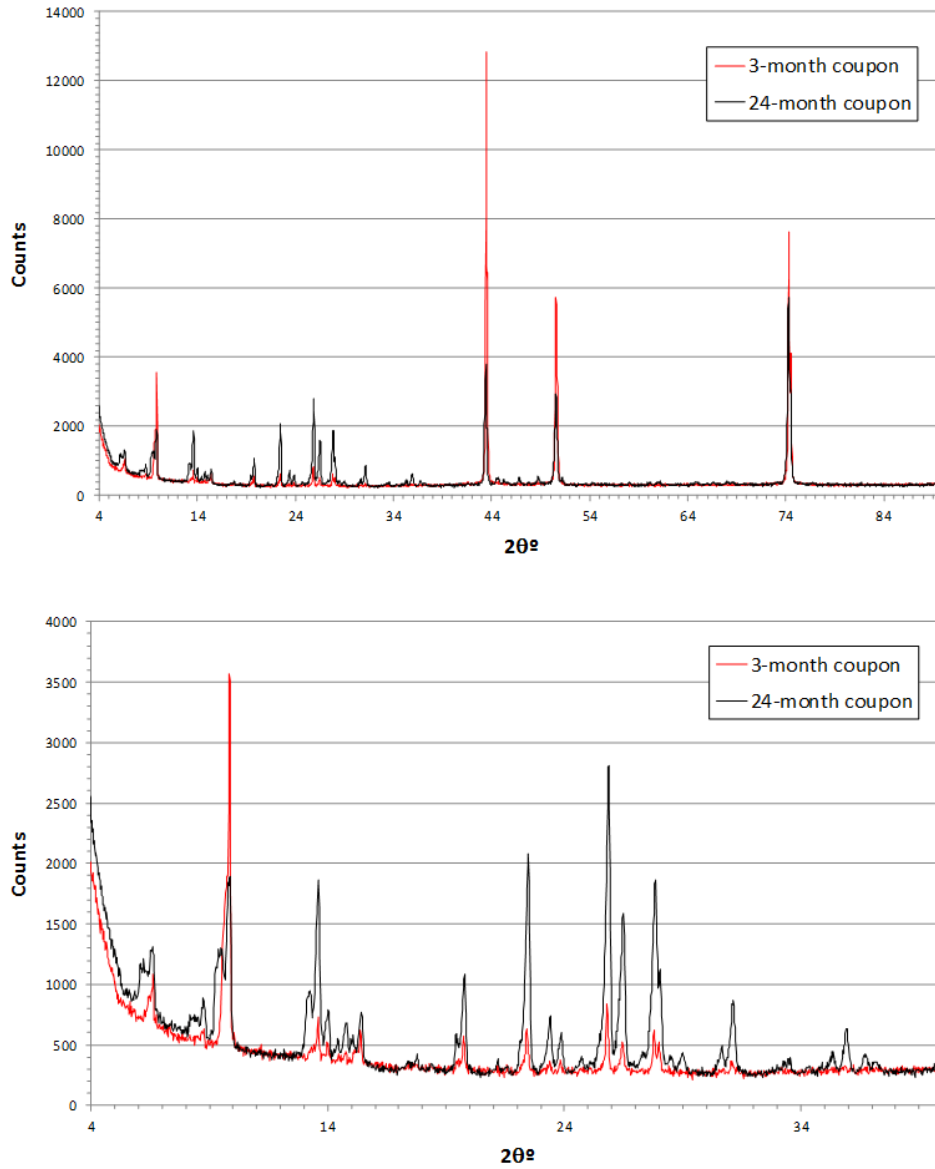


Figure 12: XRD patterns for the 3-month and 24-month SCW test coupons. Upper—full pattern from 4° to 90° 2θ. Lower—expanded view of the peaks below 40°.

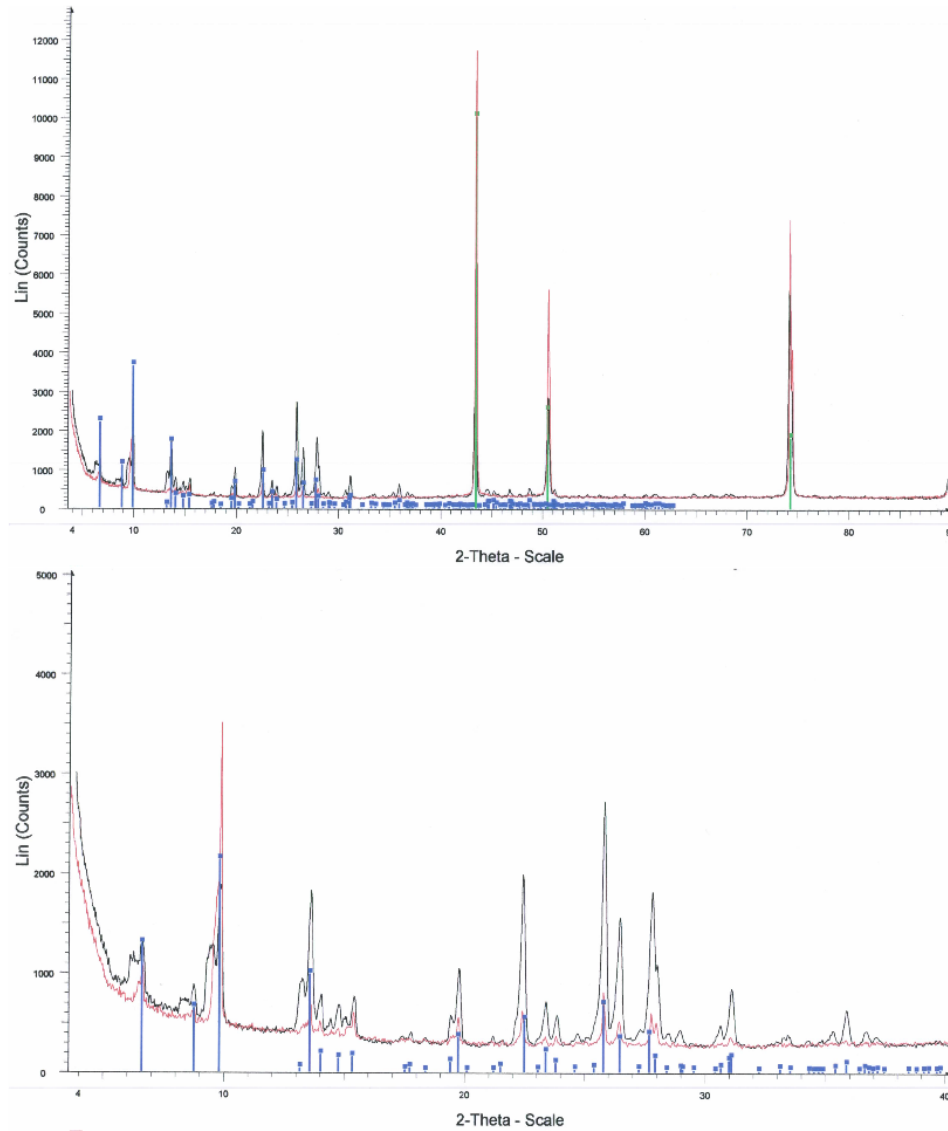


Figure 13: XRD patterns for the 3-month and 24-month SCW test coupons, along with matching phase patterns. The blue lines represent mordenite ($\text{Na}_{0.31}\text{Al}_{3.55}\text{Si}_{42.72}\text{O}_{96} \cdot 2.76 \text{H}_2\text{O}$) (Pattern 01-080-0644); the green lines represent Ni-Cr-Co-Mo (Pattern 00-035-1489), which is iso-structural to Alloy 22. Upper—full pattern from 4° to 90° 2θ. Lower—expanded view of the peaks below 40°.

Mordenite contains a trivalent ion, generally Al, in its structure, but no trivalent species is present in the nominal SCW brine. Aluminum or boron may have leached out of the glass vessel, or, alternatively, trivalent metal ions (Cr^{3+} , Fe^{3+}) may have been released by corrosion of the Alloy 22. Characterization by scanning electron microscope (SEM) with a light element energy dispersive X-ray analysis system performing energy dispersive spectroscopy (EDS) was undertaken to determine the chemical makeup of the zeolite phase. The coating is well-crystallized (Figure 14), and forms boxy orthorhombic crystals. EDS analysis (Figure 15) shows that the phase contains aluminum, as opposed to boron or other trivalent metals. Both Na and K are present in the mordenite.

During post-test sampling of the immersion test brines, a copious precipitate was observed in the elevated temperature SCW tanks. A sample of this precipitate was taken from one of the 90°C tanks. After rinsing, filtering, and drying, the sample weighed 2.8 g. The sample was estimated to represent less than 1/4 of the total precipitate, indicating that something in excess of 10 grams of material was present in the 5 liter container. XRD analysis of the sample (Figure 16) indicated that it contained both mordenite, and magadiite, a hydrous sodium silicate ($\text{Na}_2\text{Si}_{14}\text{O}_{29} \cdot 10\text{H}_2\text{O}$ is one of several proposed compositions for this phase) that precipitates as an evaporite from alkali brines. Although only 42 mg/L of silica was added to the brines (approximately 200 mg in each 5L container), several grams of silicate precipitate are present. Dissolution of the glass vessel must have been extensive over the course of the 2-year experiment.

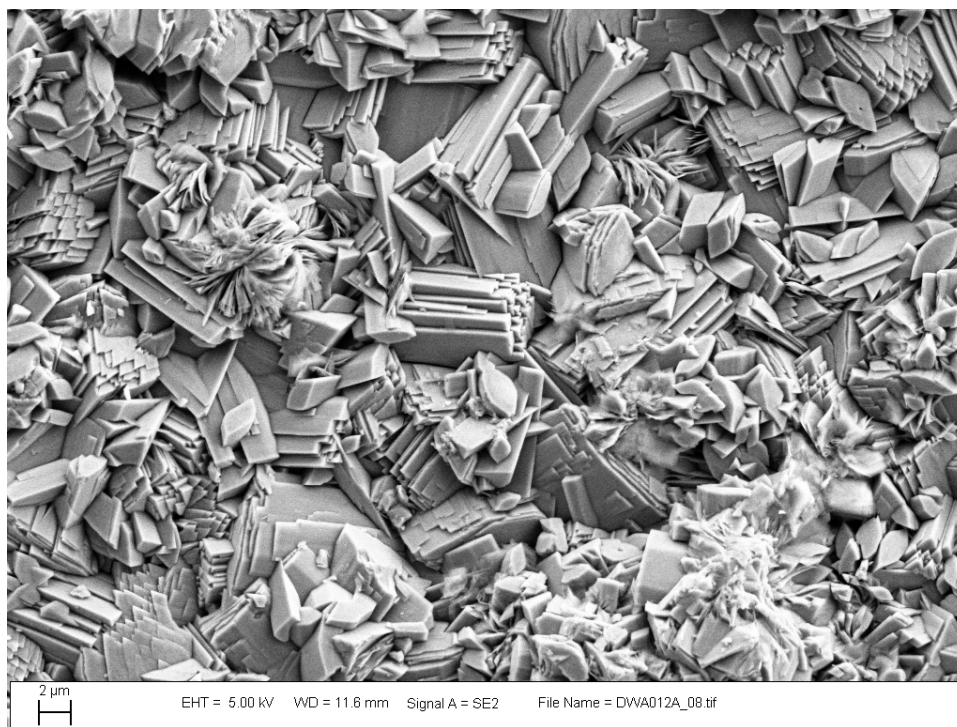


Figure 14: SEM Secondary electron image of zeolite coating on Alloy-22 coupon. The zeolite is well-crystallized, with orthorhombic crystals.

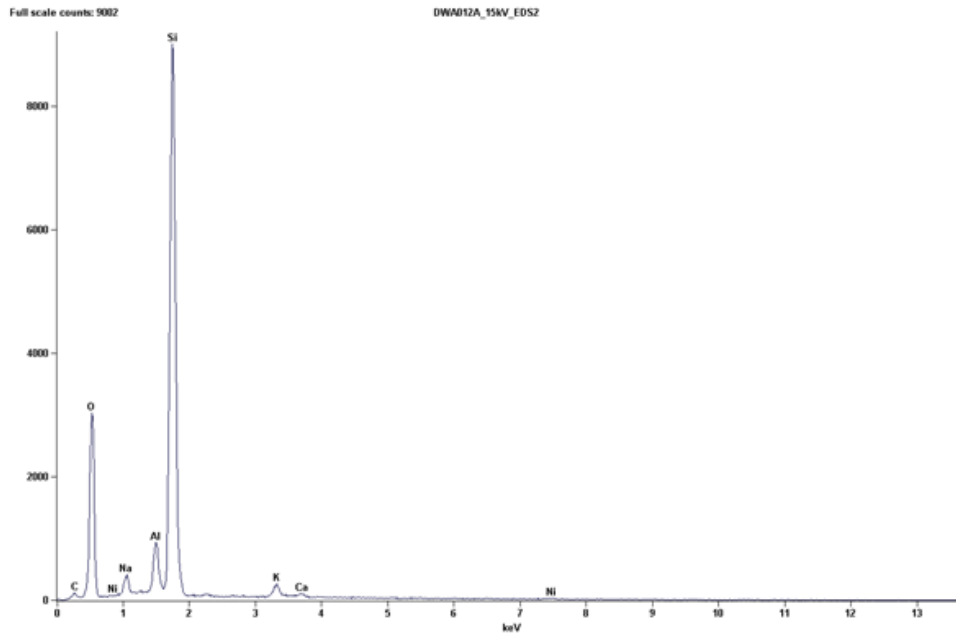


Figure 15: EDS X-ray spectrum for the crystalline coating. The material is a Na, K, Al containing mordenite.

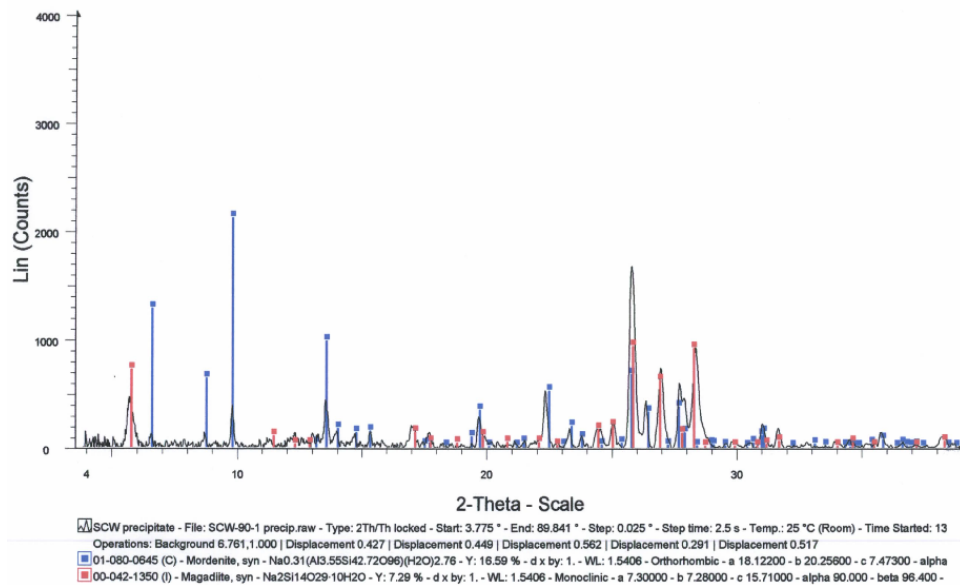


Figure 16: XRD pattern for precipitate from the SCW-90-1 reactor, along with matching phase patterns. The blue lines represent mordenite (Na_{0.31}Al_{3.55}Si_{42.72}O₉₆ • 2.76H₂O) (Pattern 01-080-0644); the red line represent magadiite (Na₂Si₁₄O₂₉ • 10H₂O) (Pattern 00-042-1350).

3.2.3 Oxide Chemistry as a Function of Temperature and Time

In a manner similar to that described in Section 3.1.4 for SAW coupons, ToF-SIMS was used to probe the composition of the oxide layer on the surface of Alloy 22 coupons taken from the SCW baths as a function of time. The ^{18}O profiles for coupons exposed to SCW as a function of temperature and time are presented in Figure 17, and the oxide thickness as a function of exposure condition and time is presented in Table 5. Once again, it should be noted that the results presented here for a single analysis area do not capture the variability which no doubt exists both within a single coupon or when comparing similar coupons.

ToF-SIMS analysis of the oxide layer also revealed that sulfur was present within the oxide for all conditions, including the ambient temperature exposure, suggesting that the material in the oxide was the result of the constituents of the exposure solution. To better illustrate the location of sulfur in regions near the metal/oxide interface, the normalized intensity of oxygen and sulfur were compared for the 24 month samples, as shown in Figure 18. The absolute concentrations of oxygen and sulfur were not determined, but the relative amount of sulfur within the oxide can clearly be seen. The large peak near about 0.3 nm depth indicates sulfur on the surface of the oxide. Despite the negligible corrosion rate for all of the samples, sulfur is observed within the oxide layer, decreasing to effectively zero at the metal/oxide interface. This observation suggests that sulfur is introduced into the oxide either through the sample preparation process, or from constituents of the exposure solution. The observation for 60°C where the oxide thickened, but the sulfur was predominantly at the surface reinforces the theory that the sulfur is due to bath constituents rather than the alloy itself.

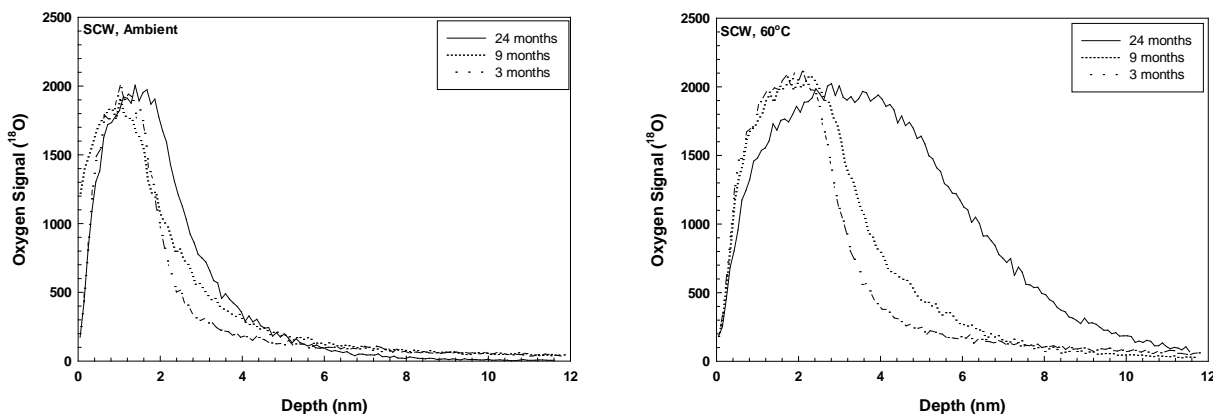


Figure 17: Oxygen-18 signal as a function of depth for Alloy 22 coupons exposed to SCW at ambient and 60°C. The 90°C samples were not analyzed due to the extensive precipitate layer present. The sharpness of the back edge of the oxygen peak indicates that the oxide is uniform, and as such the thickness was taken as the depth at which the signal was 50% of the maximum level.

Table 5: Oxide Thickness as a Function of Time in SCW

	Oxide Thickness (nm)		
	3 Months	9 Months	24 Months
Ambient	1.9	1.9	2.7
60°C	3.1	3.6	6.4
90°C	--	--	--

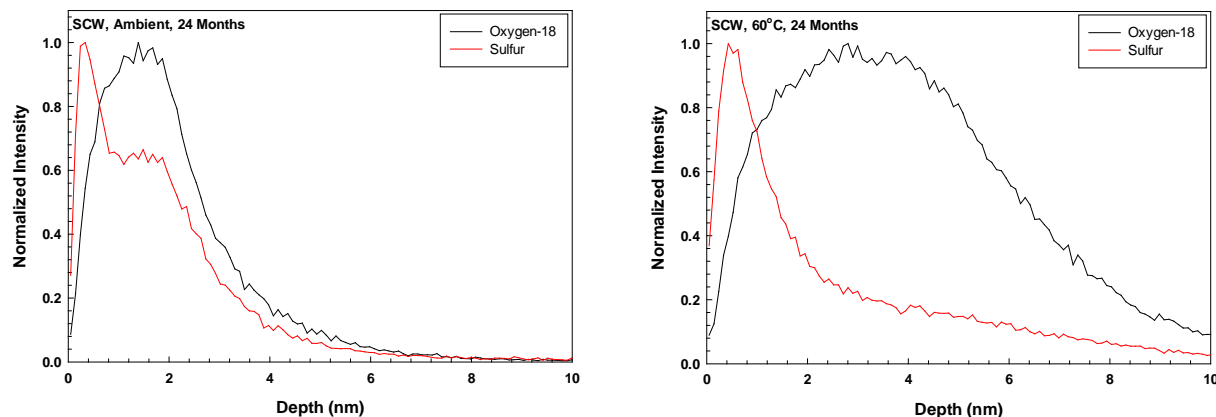


Figure 18: Comparison of the oxygen-18 and sulfur profiles through the oxide and into the metal surface for samples exposed to SCW for a period of 24 months. Data is presented as the normalized intensity for each constituent. No evidence of sulfur accumulation was observed at the metal/oxide interface for any of the samples.

3.3 0.5M NaCl

3.3.1 Weight Change as a Function of Temperature and Time

Similar to the case for SCW, based upon the Pourbaix diagram it was anticipated that Alloy 22 should be electrochemically passive in 0.5M NaCl, and as such have an extremely small dissolution rate. The resulting corrosion rates, calculated in the same manner as described above for SAW, are presented in Table 6. In all cases, the corrosion rate was effectively below the ability of the weight loss technique to detect it. A notable outlier is the data at 90°C after 9 months. Due to the geometry of the test system, the 9 month coupons were located close to the surface of the solution. In one case, the solution level dropped slightly below the top of the coupons, resulting in the formation of a dense, adherent precipitate layer on the corner of a number of the coupons. This deposit was not readily removed, and resulted in a slight weight gain for those coupons. Coupons removed at other time intervals did not have this deposit, and their calculated corrosion rate was again below the resolution of the weight-loss measurement technique. As a result, in some cases the measured value was slightly negative resulting in a negative apparent “corrosion rate”. The actual rate in such cases is effectively zero.

Table 6: Corrosion Rate vs. Time for Alloy 22 in 0.5M NaCl

	Ambient		60°C		90°C	
	CR (nm/yr)	1 SD	CR (nm/yr)	1 SD	CR (nm/yr)	1 SD
3 months	-4.6	12.8	1.8	12.7	-0.8	12.8
9 months	9.1	4.5	7.9	4.5	-50.8	4.3
18 months	1.1	2.8	2.0	2.8	2.1	2.8
24 months	-0.2	1.6	1.0	1.6	1.2	1.6

SD=standard deviation

3.3.2 Surface Morphology as a Function of Temperature and Time

Consistent with the measured weight loss for coupons exposed to 0.5M NaCl at all temperatures and time intervals, no change in the surface morphology (with the exception of the surface deposits described above for the 9 month, 90°C coupons) was observed.

3.3.3 Oxide Chemistry as a Function of Temperature and Time

ToF-SIMS ¹⁸O profiles for coupons exposed to 0.5M NaCl as a function of temperature and time are presented in Figure 19. Since the oxide layer was reasonably uniform, it was possible to determine the thickness of the oxide layer as the depth at which the signal dropped to half its maximum intensity. The oxide thickness as a function of exposure condition and time is presented in Table 7. The oxide layer thickened with time at both 60 and 90°C, consistent with the results observed for SCW at 60°C. Recalling the Pourbaix diagram (Figure 1), for a pH greater than approximately 4, chromium is not anticipated to dissolve. Thus, for both 0.5M NaCl and SCW oxide thickening would be predicted. Once again, it should be noted that the results presented here, for a single analysis area, do not capture the variability which no doubt exists both within a single coupon or when comparing similar coupons.

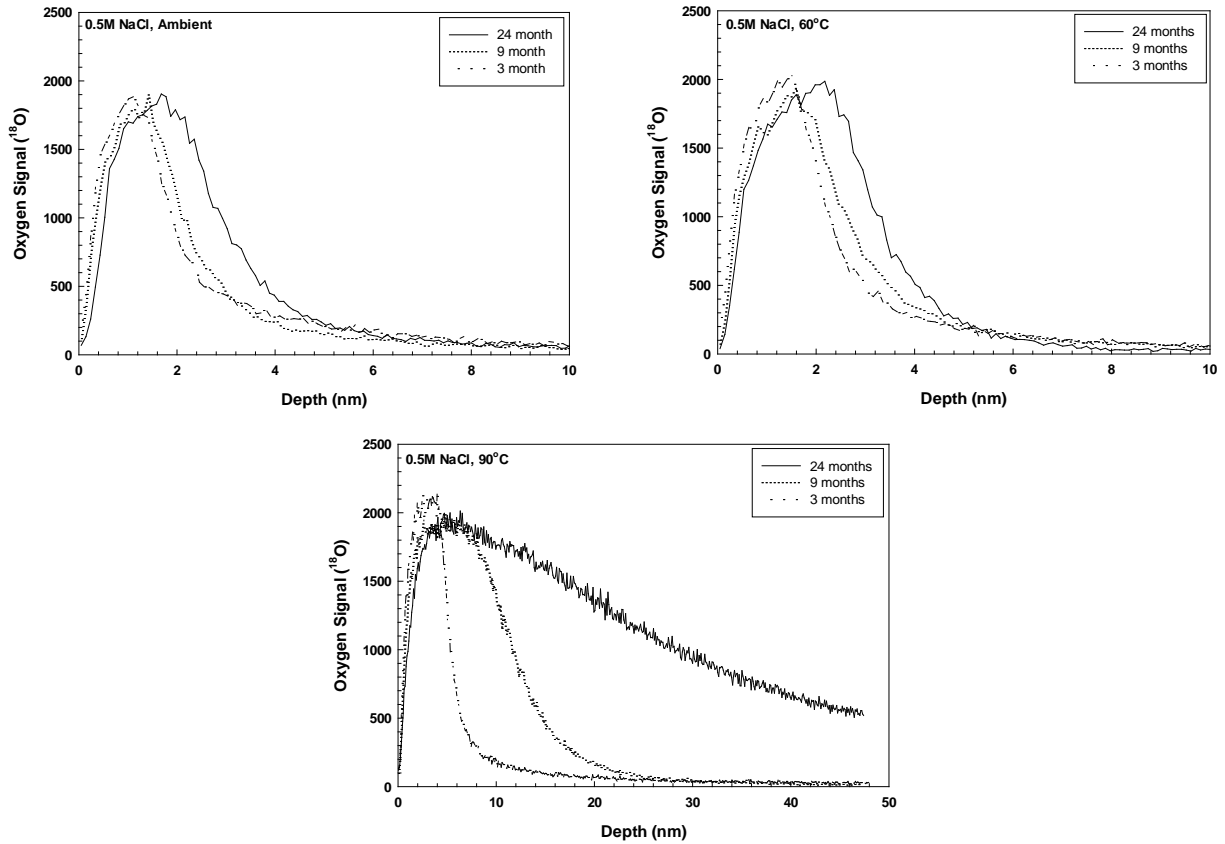


Figure 19: Oxygen-18 signal as a function of depth for Alloy 22 coupons exposed to 0.5M NaCl at ambient, 60°C, and 90°C. The sharpness of the back edge of the oxygen peak indicates that the oxide is uniform, and as such the thickness was taken as the depth at which the signal was 50% of the maximum level.

Table 7: Oxide Thickness as a Function of Time in 0.5M NaCl

	Oxide Thickness (nm)		
	3 Months	9 Months	24 Months
Ambient	2	2.1	3.1
60°C	2.3	2.7	3.3
90°C	5.5	11.9	29.3

ToF-SIMS analysis of the oxide layer also revealed that sulfur was present within the oxide for all conditions, including the ambient temperature exposure, suggesting that the material in the oxide was the result of the constituents of the exposure solution. To better illustrate the location of sulfur in regions near the metal/oxide interface, the normalized intensity of oxygen and sulfur were compared for the 24 month samples, as shown in Figure 20. The absolute concentrations of oxygen and sulfur were not determined, but the relative amount of sulfur within the oxide can clearly be seen. The large peak near about 0.3 nm depth indicates sulfur on the surface of the oxide. Despite the negligible corrosion rate for all of the samples, sulfur is observed within the oxide layer, decreasing to effectively zero at the metal/oxide interface. As the exposure solution did not contain sulfur species, the sulfur in the oxide likely originated from the specimen preparation process. This assertion is reinforced by the fact that the large peak in sulfur at the oxide surface in the SAW and SCW samples was not observed for NaCl. It should be noted that while the data for the 60°C sample appears to indicate that there was a peak at the surface, the magnitude of that peak was very small relative to the samples exposed for shorter times, and as such is likely an artifact of normalizing the data.

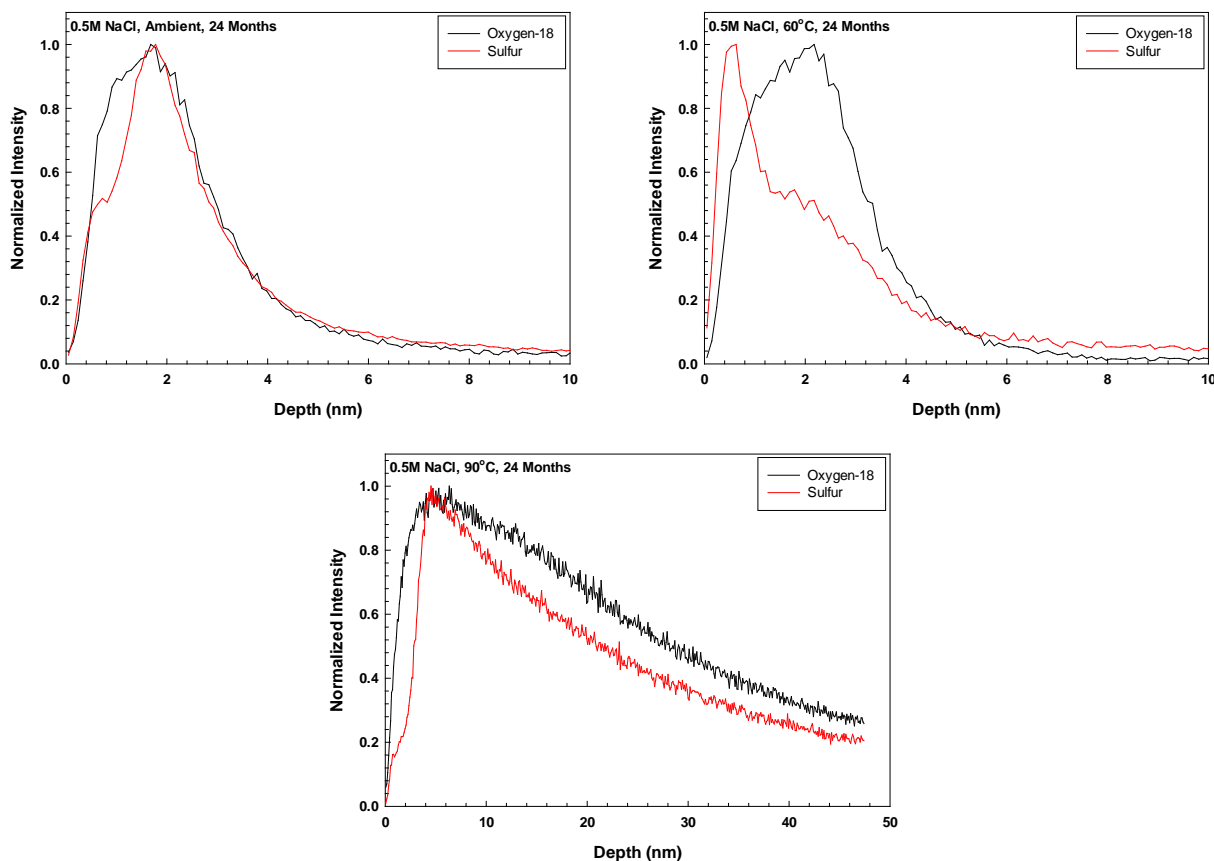


Figure 20: Comparison of the oxygen-18 and sulfur profiles through the oxide and into the metal surface for samples exposed to 0.5M NaCl for a period of 24 months. Data is presented as the normalized intensity for each constituent. No evidence of sulfur accumulation was observed at the metal/oxide interface for any of the samples.

3.4 Evolution of Solution Chemistry

Formulas for mixing the SAW, SCW, and 0.5M NaCl test solutions from simple binary salts are provided in Table 1. ACS-certified salts were used to prepare the solutions.

As discussed in Section 2.3, the brines were mixed and used to fill reactor vessels, which were maintained over the course of the 2-year experiment at the ambient lab temperature and at target temperatures of 60°C and 90°C by use of temperature-controlled heating mantles. The reactor vessels were borosilicate glass, and the 60°C and 90°C vessels were topped with chilled water condensers to reduce evaporative losses. The small amount of water that escaped the condenser was replaced with deionized water to maintain a constant solution volume. For each of the three brines, there were five vessels, one at the ambient laboratory temperature and two each at 60°C and 90°C, to allow sufficient space for samples.

Over the course of the 2-year test, visible changes were observed in some solutions. In the 60°C and 90°C SCW containers, the solutions turned cloudy, and a copious precipitate formed, especially in the 90°C containers. This precipitate was analyzed, as discussed in Section 3.2.2, and was identified as a mixture of silicates. The mass of precipitate greatly exceeded the amount of silica added to the solutions, indicating that leaching of silica from the glass vessels occurred. To assess the effect of this and other potential processes on solution composition, at the conclusion of the experiment, solution samples were taken from each of the 15 reactors and analyzed for major cations and anions. After extraction from the reactors, each sample was filtered through 0.45 µm syringe filters and split into two aliquots. The cation aliquot was acidified to 1% nitric acid, while the anion aliquot was not. It was noted that following filtering and prior to acidification, a precipitate formed in the SCW samples, and it did not re-dissolve even upon acidification to 10% HNO₃. This precipitate was a silicate, and the analyses provided here do not account for whatever brine components may have been incorporated into the solid phase.

3.4.1 SAW

Measured and nominal SAW brine compositions are given in Table 8. Major element concentrations for the SAW brines were consistent from vessel to vessel, and mostly matched the nominal values. Calcium and magnesium values were slightly lower than the nominal values, possibly indicating mineral precipitation, although no cloudiness or precipitate was observed. Finally, silica values are much higher than the nominal values, and show a consistent increase with system temperature, and there is measurable Al in these acidic brines. The silica and aluminum indicate that the glass vessels were being leached over the course of the experiment. The elevated fluoride concentration in the brine may have played a role in this process, especially in the condenser, where trace quantities of HF in the gas phase would be partitioned into the condensing fluid. The charge balance errors are a little large ($\pm 5\%$ is considered acceptable in this ionic strength range), but the data are sufficient to show that the brines are consistent with the nominal compositions.

Table 8: Nominal and Measured SAW Test Solution Compositions (mg/L)

Component	Nominal	Measured*				
		Ambient	60°C (1)	60°C (2)	90°C (1)	90°C (2)
Na ⁺	41,968	40,100	41,100	40,100	40,900	40,000
K ⁺	3,715	3,860	3,970	3,870	3,890	3,840
Ca ²⁺	80.2	71.3	59.3	59.0	55.0	53.6
Mg ²⁺	53.5	29.4	24.8	24.9	26.4	24.8
Cl ⁻	22,121	23,700	24,100	23,800	24,300	24,100
F ⁻	268	294	269	261	247	258
NO ₃ ⁻	23,750	24,700	24,900	24,600	24,900	25,000
SO ₄ ²⁻	43,534	46,000	48,000	47,700	48,600	48,000
HCO ₃ ⁻	—	NA	NA	NA	NA	NA
SiO ₂	34.1	187	267	269	381	361
Al ³⁺	—	1.78	0.52	0.52	0.47	0.46
Charge balance error, %		-4.8	-5.0	-5.7	-5.6	-6.3

NA – Not Analyzed

*in this and following tables, numbers in parenthesis correspond to which of the two baths were sampled

3.4.2 SCW

Component concentrations for the SCW brines (Table 9) were also consistent from reactor to reactor, and are largely consistent with the nominal values. However, there are some exceptions. Chloride is about twice as concentrated in the vessels as the nominal concentration indicates. It seems likely that this was due to use of HCl during acid/base pH adjustment. Although the brine formula (Table 1) is calculated to achieve the target pH, it may have been slightly off, and because the solution is strongly buffered by the high carbonate concentration, considerable acid addition is required to shift pH even slightly downward. EQ3/6 calculations show that addition of the observed 7,000-8,000 mg/L chloride as HCl would lower the pH of the brine by <0.1 pH units.

Silica concentrations are greatly elevated relative to the nominal amount, in some samples exceeding 500 mg/L. Given the large amount of silicate precipitate that also occurs in these samples (Section 3.2.2), it is clear that leaching of the glass container has occurred. This may also account for low, but measurable concentrations of Ca, Mg, and Al in the samples. Because silica solubilities increase with pH, it is not perhaps surprising that extensive glass leaching occurred in this basic solution; the elevated fluoride concentrations may also have played a role. Carbonate/bicarbonate comprise a significant fraction of the anions in these solutions and were not measured; therefore, charge balances were not calculated.

To verify that glass leaching was the cause of the elevated silica values, instead of incorrect solution preparation, archived solution samples from the SCW-60-1 (60°C bath #1) were analyzed. Three samples were analyzed, including an initial brine sample, and samples collected on 12/14/2010, and 10/19/2011. Each of the samples has precipitate in them, although the initial sample had only a minute amount. Moreover, the samples had been stored in glass vials at room temperature since collection, and were not acidified. Results of these analyses are shown in Table 10. Major element compositions match the final brine compositions closely, and vary little over the course of the experiment.

Although all of the samples contain precipitate, silica concentrations varied in each and increased with time. Also, the 10/19/2011 concentration matches almost exactly the concentration at the end of the experiment (collected in 5/2012). These observations suggest that equilibrium with the precipitate may be being maintained, and the variations in silica concentration may be due to evolution in the system pH

over time. The pH was not measured systematically, because accurate pH measurement in these brines, especially at elevated temperature, was not possible.

Table 9: Nominal and Measured SCW Test Solution Compositions (mg/L)

Component	Nominal	Measured				
		Ambient	60°C (1)	60°C (2)	90°C (1)	90°C (2)
Na ⁺	40,839	39,900	39,900	39,300	37,600	37,800
K ⁺	3,480	3,690	3,760	3,660	3,450	3,470
Ca ²⁺	—	2.46	1.38	1.40	4.13	1.91
Mg ²⁺	—	2.01	<0.2	0.21	<0.2	<0.2
Cl ⁻	6,700	14,800	13,400	13,300	12,700	12,900
F ⁻	1,254	1,230	1,240	1,230	1,170	1,190
NO ₃ ⁻	6,759	6,750	6,750	6,700	6,410	6,480
SO ₄ ²⁻	19,212	21,000	21,400	21,000	20,400	20,400
HCO ₃ ⁻	36,610	NA	NA	NA	NA	NA
SiO ₂	42.1	82	493	492	401	528
Al ³⁺	—	<0.3	<0.3	0.35	<0.3	<0.3

NA – Not Analyzed

Table 10: Measured SCW 60°C, Bath 1 Test Solution Compositions (mg/L) Through Time.

Component	Initial	12/14/2010	10/19/2011
Na ⁺	37,600	38,000	37,400
K ⁺	3,370	3,420	3,310
Ca ²⁺	1.92	1.58	1.62
Mg ²⁺	0.94	<0.2	<0.2
Cl ⁻	14,000	13,700	14,100
F ⁻	1,230	1,190	1,210
NO ₃ ⁻	6,790	6,640	6,760
SO ₄ ²⁻	21,300	20,900	21,300
HCO ₃ ⁻	NA	NA	NA
SiO ₂	60.0	383	528
Al ³⁺	<0.3	<0.3	<0.3

NA – Not Analyzed

3.4.3 0.5M NaCl

The NaCl brines (Table 11) were not uniform in concentration, although they were relatively pure NaCl brines. The NaCl concentrations varied by about a factor of five, from more dilute to more concentrated than the nominal value. Because solutions both more and less concentrated than the nominal occur, it seems likely that the variability is due to failure to completely mix the brine prior to decanting off different aliquots for use in the corrosion tests. To test this, archived solution samples of the initial brines for each tank were analyzed. As with the SCW archived samples, the samples had been stored at room temperature since collection, in glass vials. Measured component concentrations are shown in Table 12. The Na and Cl values match those of the final brine concentrations in Table 11, showing that incorrect brine preparation was indeed the cause of the variations in concentration. It is notable that measurable silica values (on the order of 20 mg/L) were recorded, indicating that during storage, even the benign NaCl brines at room temperature were capable of leaching silica from the glass vials.

Table 11: Nominal and Measured 0.5 M NaCl Test Solution Compositions (mg/L)

Component	Nominal	Measured				
		Ambient	60°C (1)	60°C (2)	90°C (1)	90°C (2)
Na ⁺	11,495	11,600	6,860	8,560	3,430	17,100
K ⁺	—	ND	ND	ND	ND	ND
Ca ²⁺	—	0.74	0.53	0.88	1.08	1.02
Mg ²⁺	—	0.25	<0.2	<0.2	<0.2	<0.2
Cl ⁻	17,725	18,500	11,100	12,800	4,990	29,700
F ⁻	—	ND	ND	ND	ND	ND
NO ₃ ⁻	—	ND	ND	ND	ND	ND
SO ₄ ²⁻	—	ND	ND	ND	ND	ND
HCO ₃ ⁻	—	NA	NA	NA	NA	NA
SiO ₂	—	6	8	99	155	162
Al ³⁺	—	<0.3	<0.3	<0.3	<0.3	<0.3
Charge balance error, %		-1.8	-2.3	1.6	2.9	-0.4

ND – Not Detected

NA– Not Analyzed

Table 12: Nominal and Measured 0.5 M NaCl Test Solution Compositions (mg/L)

Component	Concentration at initiation of experiment				
	Ambient	60°C (1)	60°C (2)	90°C (1)	90°C (2)
Na ⁺	11,300	6,870	8,320	3,480	17,200
K ⁺	ND	ND	ND	ND	ND
Ca ²⁺	0.61	0.60	0.47	0.37	0.87
Mg ²⁺	<0.2	<0.2	<0.2	<0.2	0.27
Cl ⁻	17,400	10,700	12,400	5,020	26,000
F ⁻	ND	ND	ND	ND	ND
NO ₃ ⁻	ND	ND	ND	ND	ND
SO ₄ ²⁻	ND	ND	ND	ND	ND
HCO ₃ ⁻	NA	NA	NA	NA	NA
SiO ₂	19.5	15.6	24.2	22.9	27.3
Al ³⁺	<0.3	<0.3	<0.3	<0.3	<0.3
Charge balance error, %	0.0	-0.7	1.9	3.4	1.1

ND – Not Detected

NA– Not Analyzed

Silica concentrations in the end-of-experiment NaCl brines increase with the temperature of the reactors, and the 90°C brines exceeded 150 mg/L. Again, this is attributed to leaching of the glass reactor vessels; as noted previously, even the archived samples stored at room temperature leached glass from the storage vials, so it is apparent that this phenomenon occurs readily. Low, but measurable, concentrations of Ca and Mg are probably also from glass leaching. Although carbonate and bicarbonate were not measured, they should be low relative to the background electrolyte in these near-neutral brines, and this is confirmed by the good charge balances.

In the NaCl brine tanks, the concentration of the aggressive species, chloride, varied widely. However, the maximum concentration (~0.75 M) occurred in one of the 90°C reactors, indicating that the measured corrosion rates are conservative relative to what would have been observed in 0.5 M NaCl. In any case, the measured corrosion rates were negligible—not measurably different than zero. Therefore, the variation in the brine compositions does not have an adverse impact on the interpretation of the data.

3.4.4 Summary

With one exception (chloride in SCW), measured major element concentrations of the SAW and SCW brines matched the nominal values reasonably well. Chloride concentrations in SCW are about twice the nominal value, probably due to use of HCl to adjust the solution pH to the target value. Concentrations of the NaCl brines varied widely, from well below the nominal concentration (0.5 M) to well above it. Although this affected the concentration of chloride, the corrosion-aggressive species, the observed corrosion rates should be conservative relative to the nominal (0.5 M NaCl) condition.

In all brines, silica concentrations were elevated relative to the nominal concentrations, exceeding several hundred mg/L in many cases. In the elevated temperature SCW reactors, additional silica precipitated as a mixture of silicate minerals. Several lines of evidence indicate that this was due to leaching of silica and other components from the glass reactor vessels. Given that glass leaching must have occurred, it seems likely that this is also the source for the small, but measurable, amounts of Al, Ca, and Mg in the SCW and 0.5M NaCl brines, which are nominally free of these components.

4. Discussion

4.1 Thermal Activation Energy for General Corrosion of Alloy 22

In SCW and 0.5M NaCl, the general corrosion rate for Alloy 22 observed at all temperatures and all times was below the detection limit for the weight loss test used in this study (approximately 2 nm/yr). As such, while the general corrosion rate in those environments may be observed to be a function of temperature through the use of more sensitive techniques, it was not observed in this study. In SAW, however, the general corrosion rate was clearly a function of temperature.

4.2 General Corrosion Rate of Alloy 22 as a Function of Environment, Temperature, and Time.

The dataset produced at the LTCTF for the general corrosion rate of Alloy 22 has considerable scatter to it, and the trend of the corrosion rate as a function of environment is inconsistent with any mechanistic understanding of corrosion science. In those experiments, the most aggressive condition was a slightly alkaline brine (SCW), and one of the less aggressive brines was the low pH SAW (Figure 21).

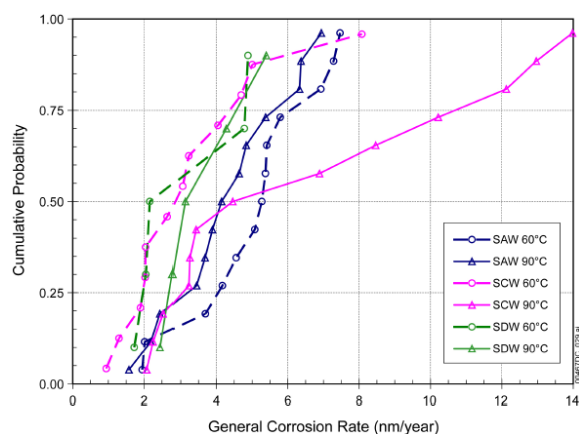


Figure 21: Corrosion Rate Distributions for 5 year Specimens in the LTCTF.

Similar to stainless steels, Alloy 22 and other Ni-Cr-X based alloys rely on the formation of a protective chromium oxide layer which forms on the metal surface. It is the durability of this passive film which dictates the general and localized corrosion behavior of such materials. Based upon the Pourbaix diagram for chromium in chloride-bearing solutions (which describes the thermodynamically stable species at a particular condition, but doesn't provide kinetic information), one would anticipate that the material would be passive at around pH 10 (SCW), but be undergoing general corrosion at pH levels below 4.5 or so. So SAW, at a pH of 2.7, would be expected to be the most aggressive, while SCW at a pH of 10, would be benign.

In addition to the counterintuitive trend in corrosion rate, the temperature dependence of the corrosion rate was also difficult to interpret from the model. Since an activation energy couldn't be extracted directly from the LTCTF data (only two temperatures, and due to the variability, there appeared to be no temperature dependence for that data) short term polarization resistance measurements were used to generate the corrosion rates as a function of temperature which in turn were used to calculate the activation energy. This polarization data also had significant scatter associated with it (multiple orders of magnitude) as illustrated in Figure 22. Because of the large degree of scatter in the datasets used to estimate the activation energy, the uncertainty was very large, and as a result, the activation energy for the model ranges from 3.37 kJ/mol to 60.05 kJ/mol.

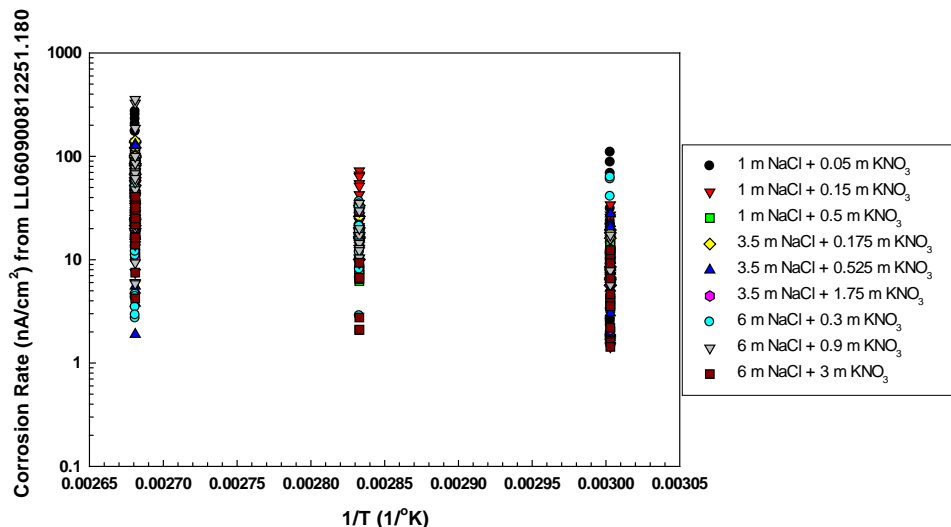


Figure 22: Corrosion rate as a function of temperature for the environments used to determine the temperature dependence of Alloy 22 in the LTCTF.

In an effort to address concerns with the data from the LTCTF, a series of long-term tests were performed on Alloy 22 in SAW, SCW, and 0.5M NaCl. Care was taken to alleviate the concerns which existed for the LLNL data (SNL, 2010) (better defined initial state, elimination of organic contamination in the bath, elimination of organic contamination from the disintegration of the containers and hardware, etc.) The corrosion rates which have resulted from those studies differ from the results obtained from the LTCTF. The corrosion rates were observed to be higher in the SAW, and virtually unmeasurable in the SCW and NaCl solutions. These results, while they are different than the results from the LTCTF, are consistent with our understanding of how Ni-Cr-Mo-W alloys behave in chloride-bearing solutions of varying pH. The results from the new testing are also very consistent, without the considerable variability exhibited by the LTCTF data.

The general corrosion rate for Alloy 22 observed in this study is summarized in Table 13 for data taken at 24 months. The corrosion behavior is clearly a strong function of environment. Under conditions where Alloy 22 is anticipated to be passive based upon the Pourbaix diagram for Cr in chloride bearing solutions, the corrosion rate was found to be vanishingly small (i.e., below the resolution of the weight loss technique as implemented in this study). However, under low pH conditions where Alloy 22 is anticipated to be active, or more specifically, where the chromium oxide passive film is not thermodynamically stable, the corrosion rate was appreciable. Furthermore, under such conditions the corrosion rate was also observed to be a strong function of temperature, with an activation energy of 72.9 ± 1.8 kJ/mol.

Table 13: 24 Month Corrosion Rate as a Function of Environment

	Ambient		60°C		90°C	
	CR (nm/yr)	1 SD	CR (nm/yr)	1 SD	CR (nm/yr)	1 SD
SAW	1.7	1.6	45.7	1.6	457.2	1.6
SCW	0.3	1.6	0*	1.6	--	--
0.5M NaCl	0*	1.6	1.0	1.6	1.2	1.6

*measured weight change slightly negative

5. Conclusions

In an effort to address concerns over the corrosion data obtained at the LTCTF, a series of long term immersion tests were performed on Alloy 22 in the same environments as were used in that study. Based upon the results obtained, the following conclusions may be made:

- The general corrosion rate of Alloy 22 is a strong function of environment, being vanishingly small in solutions where the material is passive (i.e., pH > 4.5 or so), and becoming appreciable in low pH environments, consistent with what was predicted based upon the Pourbaix diagram for Cr in chloride-bearing solutions
- Under conditions where it could be measured, the general corrosion rate of Alloy 22 was found to be a strong function of temperature, with an activation energy of 72.9 ± 1.8 kJ/mol.
- Sulfur accumulation at the metal/oxide interface was not observed for any of the conditions evaluated in this study.

6. References

Marcus, P. and Maurice, V. 2000. "Passivity of Metals and Alloys." Chapter 3 of *Corrosion and Environmental Degradation*. Schütze, M., ed. Volume I. Materials Science and Technology Volume 19. New York, New York: Wiley-VCH.

Marcus, P., ed. 2002. *Corrosion Mechanisms in Theory and Practice*. Second Edition, Revised and Expanded. Corrosion Technology 17. New York, New York: Marcel Dekker.

Pourbaix, M., 1974, *Atlas of Electrochemical Equilibria in Aqueous Solutions*, Houston, TX: NACE International.

SNL, 2007 *General Corrosion and Localized Corrosion of the Waste Package Outer Barrier*, ANL-EBS-MD-000003 Rev. 3, Albuquerque, NM: Sandia National Laboratories.

SNL, 2008a, *Technical work plan: General and localized corrosion testing of waste package and drip shield material*. TWP-WIS-MD-000022, Albuquerque, NM: Sandia National Laboratories.

SNL, 2008b, *Sample Weighing Procedure Using an Electronic Analytical Balance*, TST-PRO-T-006, Albuquerque, NM: Sandia National Laboratories

SNL, 2008c, *Cleaning Corrosion Resistant Metals Using a Hydrochloric Acid Bath*, TST-PRO-T-008, Albuquerque, NM: Sandia National Laboratories.

SNL, 2010 *Addendum to General Corrosion and Localized Corrosion of the Waste Package Outer Barrier*, ANL-EBS-MD-000003 Rev. 3 Ad. 01, Albuquerque, NM: Sandia National Laboratories.

Acknowledgements

The authors gratefully acknowledge the technical support provided by Sam Lucero for assisting with the assembly and monitoring of the exposure chambers as well as a portion of the weight change measurement, Kirsten Norman for her assistance with a portion of the weight change measurement, sample preparation, and data analysis, Carly George and Eddie Lopez for sample and solution preparation, and Alice Kilgo for her assistance with sample preparation.

Appendix 1: Mass Change Data

3 Month Data

NaCl Baths		Weight (g)					Weight Change (µg)					S.A. (cm ²)	nm/yr Corrosion Rate	nm/yr Uncertainty	
Bath T(°C)	Sample	Initial	As removed	1st clean	2nd clean	3rd clean	As removed	Cycle 1	Cycle 2	Cycle 3	Overall				Uncertainty
Ambient	ARC22-67-2	29.56652	29.56653	29.56653	29.56653	29.56654	0	0	0	-10	-10	0.00003	28.7	-1.6	4.8
	ARC22-69-1	29.34997	29.35002	29.35000	29.35001	29.35000	-50	10	-10	10	-40	0.00003	28.1	-6.6	4.9
	ARC22-77-2	29.71771	29.71769	29.71773	29.71776	29.71770	20	-40	-30	60	10	0.00003	28.3	1.6	4.9
	ARC22-79-2	30.40872	30.40872	30.40875	30.40877	30.40872	0	-30	-20	50	0	0.00003	28.5	0.0	4.8
	ARC22-87-2	29.60075	29.60076	29.60081	29.60082	29.60077	0	-60	0	50	-10	0.00003	28.2	-1.6	4.9
	DCA288-1	30.87689	30.87693	30.87695	30.87692	30.87695	-40	-20	30	-30	-70	0.00003	29.1	-11.1	4.7
	DCA315-2	30.44301	30.44305	30.44307	30.44304	30.44309	-50	-20	40	-50	-80	0.00003	28.9	-12.7	4.8
60C (1)															
	ARC22-73-2	29.62407	29.62402	29.62409	29.62404	29.62405	50	-70	50	-10	20	0.00003	28.4	3.2	4.9
	DCA285-2	30.23173	30.23177	30.23180	30.23177	30.23175	-30	-30	30	20	-20	0.00003	28.6	-3.2	4.8
	DCA292-1	30.50870	30.50863	30.50864	30.50862	30.50865	70	-20	30	-30	50	0.00003	28.8	8.0	4.8
60C (2)	ARC22-73-1	29.67796	29.67790	29.67790	29.67797	29.67794	60	0	-70	30	20	0.00003	28.7	3.2	4.8
	ARC22-90-1	30.44313	30.44308	30.44311	30.44310	30.44311	50	-30	-10	-10	20	0.00003	28.8	3.2	4.8
	DCA290-2	30.13277	30.13277	30.13275	30.13280	30.13277	0	20	-50	30	0	0.00003	28.9	0.0	4.8
	DCA291-2	30.39733	30.39733	30.39732	30.39739	30.39735	0	10	-70	40	-10	0.00003	28.9	-1.6	4.8
90C (1)															
	ARC22-89-2	29.05749	29.05756	29.05758	29.05752	29.05753	-80	-20	60	-10	-50	0.00003	28.0	-8.2	4.9
	DCA287-1	30.57615	30.57621	30.57619	30.57619	30.57621	-60	20	-10	-10	-60	0.00003	29.1	-9.5	4.7
	DCA289-1	30.11289	30.11284	30.11284	30.11288	30.11285	50	0	-40	30	40	0.00003	28.8	6.4	4.8
90C (2)	ARC22-71-2	29.82146	29.82147	29.82146	29.82147	29.82148	-10	10	-10	-10	-20	0.00003	28.4	-3.2	4.9
	ARC22-76-2	29.86254	29.86257	29.86257	29.86253	29.86257	-20	-10	50	-50	-30	0.00003	28.2	-4.9	4.9
	DCA285-1	30.70819	30.70813	30.70811	30.70809	30.70805	60	20	20	40	140	0.00003	29.2	22.1	4.7
	DCA293-2	29.89534	29.89539	29.89539	29.89539	29.89539	-50	0	0	0	-50	0.00003	28.9	-8.0	4.8

SCW Baths		Weight (g)						Weight Change (µg)					S.A. (cm ²)	nm/yr Corrosion Rate	nm/yr Uncertainty		
Bath T(°C)	Sample	Initial	As removed	1st clean	2nd clean	3rd clean	4th clean	As removed	Cycle 1	Cycle 2	Cycle 3	Cycle 4				Overall	Uncertainty
Ambient	ARC22-66-1	29.10444	29.10443	29.10443	29.10444	29.10444	29.10444	10	10	-10	0	10	10	0.00003	28.7	2	4.8
	ARC22-69-2	30.05061	30.05062	30.05064	30.05061	30.05064	30.05061	-10	-30	30	-20	30	0	0.00003	28.3	0	4.9
	ARC22-77-1	30.27604	30.27601	30.27599	30.27605	30.27604	30.27602	20	20	-60	10	20	10	0.00003	28.5	2	4.8
	ARC22-85-1	29.40249	29.40248	29.40252	29.40251	29.40251	29.40251	10	-40	20	0	0	-10	0.00003	28.2	-2	4.9
	DCA287-2	30.03313	30.03313	30.03316	30.03315	30.03316	30.03316	0	-30	10	-10	0	-30	0.00003	29.1	-5	4.7
	DCA288-2	30.04010	30.04007	30.04010	30.04007	30.04011	30.04008	30	-30	30	-40	30	20	0.00003	28.7	3	4.8
	DCA293-1	30.03514	30.03514	30.03518	30.03515	30.03517	30.03514	0	-30	30	-20	30	0	0.00003	28.9	0	4.8
60C (1)	ARC22-71-1	30.53265	30.53263	30.53265	30.53267	30.53265	30.53266	20	-20	-20	20	-10	-10	0.00003	28.4	-2	4.9
	ARC22-75-1	30.66920	30.66913	30.66915	30.66917	30.66916	30.66917	60	-20	-20	10	-10	30	0.00003	28.4	5	4.9
	DCA294-2	30.75925	30.75927	30.75928	30.75925	30.75926	30.75930	-20	0	30	-20	-40	-50	0.00003	28.8	-8	4.8
60C (2)	ARC22-67-1	29.60219	29.60219	29.60226	29.60224	29.60222	29.60225	10	-70	20	20	-30	-60	0.00003	28.7	-10	4.8
	ARC22-76-1	30.82795	30.82793	30.82794	30.82798	30.82794	30.82796	20	-10	-40	30	-20	-20	0.00003	28.8	-3	4.8
	DCA289-2*	29.83360	29.83359	29.83356	29.83352	29.83346	29.83344	10	30	30	60	20	160	0.00003	28.9	25	4.8
	DCA315-1	30.17387	30.17386	30.17388	30.17389	30.17386	30.17387	10	-30	-10	30	-10	-10	0.00003	28.9	-2	4.8
90C (1)																	
	ARC22-74-1	30.35296	30.35914	30.35836				-6190	790				-5400	#DIV/0!	28.0	-888	
	DCA286-2	30.28435	30.28993	30.28946				-5580	470				-5110	#DIV/0!	29.1	-808	
	DCA294-1	30.67328	30.68003	30.67906				-6740	970				-5780	#DIV/0!	28.8	-924	
90C (2)	ARC22-64-2	28.76096	28.76242	28.76171				-1460	710				-750	#DIV/0!	28.4	-122	
	ARC22-74-2	29.96975	29.97088	29.97030				-1120	570				-550	#DIV/0!	28.2	-90	
	ARC22-78-1	31.02661	31.02906	31.02739				-2450	1670				-790	#DIV/0!	29.2	-125	
	DCA316-2	30.45968	30.46489	30.46090				-5210	3990				-1220	#DIV/0!	28.9	-194	

SAW Baths		Weight (g)					Weight Change (µg)					S. A. (cm ²)	nm/yr Corrosion Rate	nm/yr Uncertainty	
Bath T(°C)	Sample	Initial	As removed	1st clean	2nd clean	3rd clean	As removed	Cycle 1	Cycle 2	Cycle 3	Overall				Uncertainty
Ambient	ARC22-63-1	29.97608	29.97608	29.97612	29.97609	29.97612	0	-40	20	-20	-30	0.00003	28.7	-5	4.8
												0.00002			
	ARC22-64-1	32.00241	32.00240	32.00249	32.00240	32.00248	10	-90	90	-80	-70	0.00003	28.3	-11	4.9
	ARC22-65-1	30.96545	30.96546	30.96549	30.96545	30.96549	-10	-30	40	-40	-40	0.00003	28.5	-6	4.8
	ARC22-70-2	28.07476	28.07475	28.07483	28.07479	28.07479	10	-80	40	0	-30	0.00003	28.2	-5	4.9
	ARC22-78-2	30.12943	30.12939	30.12937	30.12938	30.12939	40	20	-10	-20	40	0.00003	29.1	6	4.7
	ARC22-86-1	30.14790	30.14786	30.14791	30.14786	30.14788	50	-60	50	-10	30	0.00003	28.7	5	4.8
DCA286-1	30.36075	30.36077	30.36078	30.36073	30.36081	-20	-10	50	-70	-60	0.00003	28.9	-10	4.8	
60C (1)	ARC22-62-2	29.95566	29.95525	29.95526	29.95526	29.95528	420	-10	0	-20	380	0.00003	28.4	62	4.9
	ARC22-72-1	29.85465	29.85429	29.85431	29.85429	29.85431	370	-30	20	-20	340	0.00003	28.6	55	4.8
	ARC22-88-1	30.70581	30.70529	30.70531	30.70528	30.70525	520	-20	30	20	560	0.00003	28.8	90	4.8
60C (2)	ARC22-68-1	29.42062	29.42024	29.42021	29.42023	29.42024	380	30	-20	-10	390	0.00003	28.7	63	4.8
	ARC22-80-1	30.75249	30.75215	30.75211	30.75213	30.75212	340	40	-20	0	370	0.00003	28.8	59	4.8
	ARC22-80-2	30.42933	30.42890	30.42893	30.42893	30.42894	430	-30	0	-10	390	0.00003	28.9	62	4.8
	DCA316-1	30.94267	30.94232	30.94232	30.94232	30.94231	350	0	0	10	360	0.00003	28.9	57	4.8
90C (1)	ARC22-79-1	30.63188	30.62873	30.62865	30.62867	30.62867	3160	80	-20	0	3220	0.00003	28.1	527	4.9
	ARC22-85-2	31.23630	31.23309	31.23301	31.23300	31.23300	3210	70	20	0	3300	0.00003	28.0	542	4.9
	ARC22-88-2	29.92251	29.91945	29.91944	29.91944	29.91945	3060	0	10	-20	3050	0.00003	29.1	482	4.7
90C (2)	ARC22-68-2	29.63211	29.62903	29.62901	29.62904	29.62902	3080	20	-30	20	3080	0.00003	28.4	499	4.9
	ARC22-87-1	30.12182	30.11872	30.11909	30.11875	30.11876	3100	-370	340	-10	3050	0.00003	28.2	498	4.9
	DCA290-1	30.98573	30.98261	30.98262	30.98262	30.98264	3120	-10	0	-20	3080	0.00003	29.2	486	4.7
	DWA166A	23.14109	23.13824	23.13822	23.13820	23.13820	2850	20	20	0	2890	0.00003	28.9	460	4.8

9 Month Data

NaCl Baths		Weight (g)					Weight Change (µg)				Overall Change (µg)	Overall Uncertainty	S.A. (cm ²)	Corrosion Rate (nm/yr)	Uncertainty nm/yr
Bath T(°C)	Sample	Initial	As removed	1st clean	2nd clean	3rd clean	As removed	Cycle 1	Cycle 2	Cycle 3					
Ambient	ARC22-42-2	25.84029	25.84028	25.84021	25.84023	25.84022	10	70	-30	10	70	0.00003	27.1	4	1.7
	DWB114A	11.40430	11.40419	11.40419	11.40421	11.40406	110	0	-20	150	240	0.00003	26.5	14	1.7
	DWB115A	12.65183	12.65172	12.65144	12.65174	12.65172	110	280	-290	20	110	0.00003	26.7	6	1.7
	DWB121A	21.20581	21.20549	21.20577	21.20580	21.20558	320	-280	-30	220	230	0.00003	27.8	13	1.7
	DWB122A	17.91831	17.91798	17.91825	17.91824	17.91799	330	-270	10	250	320	0.00003	27.3	18	1.7
	DWB123A	13.12233	13.12229	13.12229	13.12228	13.12227	40	0	10	10	50	0.00003	26.8	3	1.7
	DWB124A	21.67329	21.67327	21.67323	21.67321	21.67318	20	40	20	40	110	0.00003	28.1	6	1.6
60C (1)	ARC22-44-2	27.80246	27.80237	27.80231	27.80233	27.80230	90	70	-20	20	160	0.00003	28.7	9	1.6
	ARC22-45-2	27.80987	27.80980	27.80975	27.80972	27.80979	70	60	30	-70	80	0.00003	28.5	4	1.6
	DCA309-2	28.99024	28.99015	28.99005	28.99002	28.99000	90	100	30	20	240	0.00003	28.0	13	1.6
60C (2)	ARC22-57-1	27.12873	27.12869	27.12859	27.12861	27.12863	30	110	-30	-20	100	0.00003	27.8	6	1.7
	ARC22-58-1	28.63330	28.63325	28.63319	28.63282	28.63316	50	60	370	-340	140	0.00004	29.2	7	2.1
	DCA305-2	28.36484	28.36473	28.36462	28.36463	28.36461	110	110	-10	20	230	0.00003	28.1	13	1.6
	DWB006A	24.18981	24.18975	24.18973	24.18977	24.18974	60	30	-40	30	70	0.00003	28.3	4	1.6
90C (1)	ARC22-41-1	26.07402	26.07623	26.07570	26.07564	26.07563	-2220	530	60	10	-1610	0.00003	27.6	-90	1.7
	ARC22-42-1	28.39721	28.39707	28.39708	28.39705	28.39704	150	-10	30	20	180	0.00003	28.9	10	1.6
	ARC22-43-1	26.03964	26.04142	26.04089	26.04068	26.04072	-1770	530	210	-40	-1070	0.00003	27.6	-59	1.7
	ARC22-44-1	25.39360	25.39556	25.39497	25.39487	25.39487	-1960	590	50	50	-1270	0.00003	27.5	-71	1.7
90C (2)	ARC22-50-2	27.00417	27.00481	27.00480	27.00482	27.00479	-640	0	-20	30	-620	0.00003	28.2	-34	1.6
	ARC22-51-2	26.97520	26.97589	26.97587	26.97588	26.97585	-700	20	-10	30	-660	0.00003	28.3	-36	1.6
	DCA304-1	28.18557	28.18708	28.18702	28.18693	28.18695	-1510	60	100	-20	-1380	0.00003	28.0	-76	1.6

SCW Baths		Weight (g)					Weight Change (µg)				Overall Change (µg)	Overall Uncertainty	S.A. (cm ²)	Corrosion Rate (nm/yr)	Uncertainty nm/yr
Bath T(°C)	Sample	Initial	As removed	1st clean	2nd clean	3rd clean	As removed	Cycle 1	Cycle 2	Cycle 3					
Ambient	ARC22-48-2	27.75950	27.75930	27.75936	27.75939	27.75932	200	-60	-30	70	170	0.00004	28.6	9.1	2.1
	DWA002A	26.32110	26.32101	26.32102	26.32102	26.32100	90	0	0	20	100	0.00003	29.0	5.3	1.6
	DWA003A	26.04740	26.04735	26.04731	26.04733	26.04729	50	40	-30	40	110	0.00003	28.9	5.8	1.6
	DWA153A	23.55530	23.55521	23.55518	23.55515	23.55512	90	30	30	20	170	0.00003	28.5	9.2	1.6
	DWA168A	22.26748	22.26735	22.26741	22.26734	22.26711	130	-50	70	230	370	0.00003	28.0	20.3	1.6
	DWB087A	20.90546	20.90532	20.90536	20.90531	20.90528	140	-40	50	30	180	0.00003	26.9	10.3	1.7
	DWB088A	21.14335	21.14326	21.14322	21.14322	21.14321	90	40	0	10	140	0.00003	27.9	7.7	1.6
60C (1)	ARC22-52-2	26.27398	26.27397	26.27390	26.27386	26.27383	10	70	40	30	150	0.00003	27.8	8.3	1.7
	DCA312-2	28.77142	28.77136	28.77124	28.77122	28.77127	60	120	20	-50	150	0.00003	28.0	8.2	1.6
	DWB085A	17.68039	17.68041	17.68034	17.68030	17.68033	-20	80	30	-30	60	0.00003	28.5	3.2	1.6
60C (2)	DCA312-1	28.77670	28.77668	28.77657	28.77654	28.77657	20	110	20	-30	130	0.00003	28.4	7.0	1.6
	DWA111A	25.37488	25.37504	25.37498	25.37485	25.37489	-150	60	130	-40	0	0.00003	28.8	0.0	1.6
	DWA112A	25.87726	25.87747	25.87733	25.87726	25.87726	-210	140	70	0	0	0.00003	28.7	0.0	1.6
	DWB075A	22.36110	22.36118	22.36108	22.36103	22.36102	-90	110	40	10	80	0.00003	28.2	4.4	1.6
90C (1)	ARC22-55-2	26.57863	26.57877	26.57868	26.57859	26.57864	-140	90	90	-40	-10	0.00003	28.3	-0.5	1.6
	DCA311-1	29.00475	29.00546	29.00493	29.00471	29.00469	-710	540	210	20	60	0.00003	28.6	3.2	1.6
	DWA073A	25.50666	25.50705	25.50686	25.50674	25.50674	-390	190	120	10	-80	0.00003	29.0	-4.2	1.6
	DWB044A	23.91499	23.91518	23.91511	23.91502	23.91504	-190	70	90	-20	-50	0.00003	28.3	-2.7	1.6
90C (2)	ARC22-59-1	27.00554	27.00564	27.00556	27.00549	27.00551	-100	90	70	-30	20	0.00003	28.3	1.1	1.6
	DWA103A	22.87918	22.87953	22.87943	22.87933	22.87933	-360	100	100	0	-160	0.00003	28.6	-8.6	1.6
	DWB055A	21.61649	21.61671	21.61666	21.61664	21.61663	-220	50	30	10	-140	0.00003	27.4	-7.8	1.7

Final Report: Immersion Tests to Evaluate Corrosion of Alloy 22 in Heated Brine Solutions

SAW Baths		Weight (g)					Weight Change (µg)				Overall Change (µg)	Overall Uncertainty	S.A. (cm ²)	Corrosion Rate (nm/yr)	Uncertainty nm/yr	
Bath T(°C)	Sample	Initial	As removed	1st clean	2nd clean	3rd clean	As removed	Cycle 1	Cycle 2	Cycle 3						
Ambient	ARC22-54-2	25.78166	25.78157	25.78152	25.78154	25.78151	80	50	-20	30	150	0.00003	28.0	8	1.6	
	DWA088A	23.07897	23.07888	23.07876	23.07882	23.07881	90	120	-60	10	160	0.00003	28.5	9	1.6	
	DWA106A	26.31657	26.31651	26.31641	26.31642	26.31643	60	110	-20	-10	140	0.00003	29.0	7	1.6	
	DWA169A	20.58898	20.58899	20.58888	20.58888	20.58887	-10	110	0	20	120	0.00003	27.7	7	1.7	
	DWB011A	21.25980	21.25976	21.25973	21.25974	21.25971	40	30	-10	30	90	0.00003	27.9	5	1.6	
	DWB012A	22.20092	22.20088	22.20086	22.20087	22.20083	40	20	-10	30	90	0.00003	28.1	5	1.6	
	DWB015A	11.24204	11.24203	11.24197	11.24200	11.24200	10	60	-30	10	40	0.00003	26.9	2	1.7	
60C (1)	DCA313-1	28.85916	28.85801	28.85796	28.85798	28.85794	1160	50	-20	40	1230	0.00003	28.9	65	1.6	
	DWA001A	25.78335	25.78240	25.78247	25.78244	25.78246	950	-70	30	-20	900	0.00003	28.4	49	1.6	
	DWA055A	22.79628		22.79548	22.79548	22.79549			0	-10	790	0.00003	28.6	42	1.6	
60C (2)	DCA308-1	30.64210	30.64118	30.64099	30.64098	30.64097	910	200	10	10	1120	0.00003	28.7	60	1.6	
	DWA038A	22.07247	22.07178	22.07172	22.07172	22.07172	690	60	0	-10	750	0.00003	28.3	41	1.6	
	DWB038A	17.60972	17.60902	17.60900	17.60899	17.60902	700	20	10	-30	700	0.00003	28.4	38	1.6	
	DWB041A	22.20810	22.20738	22.20711	22.20735	22.20736	720	280	-250	-10	730	0.00003	27.7	40	1.7	
90C (1)	DWA036A	25.76867	25.75987	25.75971	25.75972	25.75973	8800	160	0	-20	8940	0.00003	28.6	480	1.6	
	DWA115A	21.58636	21.57777	21.57771	21.57767	21.57768	8580	60	40	-10	8670	0.00003	28.9	460	1.6	
	DWA116A	23.45757	23.44876	23.44861	23.44865	23.44862	8820	150	-50	40	8960	0.00003	28.5	482	1.6	
	DWB103A	21.60213	21.59362	21.59363	21.59364	21.59362	8510	-10	0	20	8520	0.00003	28.1	465	1.6	
90C (2)	DWA122A	21.82127	21.81232	21.81230	21.81229	21.81226	8950	20	10	30	9010	0.00003	28.3	488	1.6	
	DWA123A	22.16190	22.15336	22.15341	22.15342	22.15341	8540	-50	0	10	8490	0.00003	27.5	474	1.7	
	DWB169A	21.38698	21.37858	21.37830	21.37824	21.37823	8410	280	60	10	8750	0.00003	28.0	479	1.6	

18 Month Data

NaCl Baths		Weight (g)					Weight Change (µg)					Overall	Overall	S.A. (cm ²)	Corrosion	Uncertainty
Bath T(°C)	Sample	Initial	As removed	1st clean	2nd clean	3rd clean	As removed	Cycle 1	Cycle 2	Cycle 3	Cy1-Cy3	Change (µg)	Uncertainty		Rate (nm/yr)	nm/yr
Ambient	ARC22-45-1	26.63005	26.63002	26.62997		26.62998	30	50			-10	70	0.00003	28.4	1.9	0.8
	ARC22-46-1	27.71373	27.71367	27.71367		27.71372	60	0			-50	10	0.00003	29.6	0.3	0.8
	DCA295-2	28.84937	28.84928	28.84924		28.84929	90	40			-50	80	0.00003	29.0	2.1	0.8
	DCA296-2	29.85972	29.85967	29.85959		29.85964	50	80			-50	80	0.00003	29.2	2.1	0.8
	DCA313-2	28.60583	28.60579	28.60575		28.60579	40	40			-40	40	0.00003	28.9	1.1	0.8
	DCA314-2	28.71391	28.71387	28.71384		28.71387	40	30			-30	40	0.00003	29.1	1.1	0.8
	DWB116A	21.34233	21.34231	21.34230		21.34231	20	10			-10	20	0.00003	28.4	0.5	0.8
	DWB118A	22.56517	22.56518	22.56513		22.56516	-10	50			-30	10	0.00003	28.7	0.3	0.8
										0						
60C (1)	ARC22-60-2	27.18086	27.18076	27.18069	27.18077	27.18074	100	70	-80	30	-50	120	0.00003	29.0	3.2	0.8
	ARC22-61-2	26.33281	26.33270	26.33264	26.33264	26.33268	110	60	0	-40	-40	130	0.00003	28.7	3.5	0.8
	DWB003A	22.35273	22.35274	22.35271		22.35272	-10	30			-10	10	0.00003	28.8	0.3	0.8
	DWB004A	23.70622	23.70617	23.70610		23.70616					-60		0.00003	29.0	0.0	0.8
60C (2)	DCA296-1	30.00312	30.00304	30.00302	30.00298	30.00301	80	20	40	-30	10	110	0.00003	29.6	2.9	0.8
	DCA297-1	29.13613	29.13608	29.13599	29.13600	29.13603	50	90	-10	-30	-40	100	0.00003	29.1	2.6	0.8
	DCA302-1	28.96197	28.96193	28.96185	28.96190	28.96189	40	80	-50	10	-40	80	0.00003	28.8	2.1	0.8
	DWB005A	22.09857	22.09853	22.09850	22.09850	22.09851	40	30	0	-10	-10	60	0.00003	28.6	1.6	0.8
90C (1)	DCA297-2	28.96067	28.96057	28.96053	28.96056	28.96055	100	40	-30	10	-20	120	0.00003	29.2	3.2	0.8
	DWA004A	26.10334	26.10326	26.10322	26.10325	26.10324	80	40	-30	10	-20	100	0.00003	29.5	2.6	0.8
	DWA005A	25.19855	25.19848	25.19843	25.19847	25.19845	70	50	-40	20	-20	100	0.00003	29.5	2.6	0.8
	DWA008A	24.31241	24.31236	24.31229	24.31235	24.31234					-50		0.00003	29.4	0.0	0.8
90C (2)	ARC22-49-1	25.55364	25.55351	25.55347		25.55353	130	40			-60	110	0.00003	28.6	3.0	0.8
	ARC22-52-1	25.14193	25.14179	25.14173		25.14178	140	60			-50	150	0.00003	28.0	4.1	0.8
	DWA009A	22.84845	22.84842	22.84837		22.84841	30	50			-40	40	0.00003	29.0	1.1	0.8
	DWB125A	12.87414	12.87416	12.87415	12.87414	12.87415	-20	10	10	-10	0	-10	0.00003	27.2	-0.3	0.8

SCW Baths		Weight (g)					Weight Change (µg)					Overall	Overall	S.A. (cm ²)	Corrosion	Uncertainty	
Bath T(°C)	Sample	Initial	As removed	1st clean	2nd clean	3rd clean	As removed	Cycle 1	Cycle 2	Cycle 3	Cy1-Cy3	Change (µg)	Uncertainty		Rate (nm/yr)	nm/yr	
Ambient	DWA142A	24.26575	24.26577	24.26575		24.26575	-20	20			0	0	0.00003	29.4	0.0	0.8	
	DWA143A	24.26910	24.26918	24.26912		24.26910	-80	60			20	0	0.00003	29.2	0.0	0.8	
	DWA146A	22.03945	22.03955	22.03949	22.03949	22.03946	-100	60	0	30	30	-10	0.00003	28.8	-0.3	0.8	
	DWA164A	24.46738	24.46739	24.46740		24.46740	-10	-10			0	-20	0.00003	28.8	-0.5	0.8	
	DWB046B	12.94502	12.94512	12.94505	12.94506	12.94504	-100	70	-10	20	10	-20	0.00003	27.0	-0.6	0.9	
	DWB081A	23.22040	23.22045	23.22039	23.22041	23.22042	-50	60	-20	-10	-30	-20	0.00003	28.9	-0.5	0.8	
											0						
	DWB111A	18.55021	18.55027	18.55024		18.55024	-60	30			0	-30	0.00003	27.9	-0.8	0.8	
										0							
60C (1)	DWA079A	22.43127	22.43135	22.43133		22.43135	-80	20			-20	-80	0.00003	28.9	-2.1	0.8	
	DWA113A	24.62218	24.62237	24.62238		24.62236	-190	-10			20	-180	0.00003	29.4	-4.7	0.8	
	DWB076A	22.50734	22.50741	22.50741		22.50742	-70	0			-10	-80	0.00003	28.7	-2.1	0.8	
	DWB084A	18.16890	18.16898	18.16900		18.16897	-80	-20			30	-70	0.00003	28.0	-1.9	0.8	
										0							
60C (2)	ARC22-50-1	26.52796	26.52791	26.52789		26.52791	50	20			-20	50	0.00003	28.2	1.4	0.8	
	DWA082A	24.33939	24.33942	24.33939		24.33943	-30	30			-40	-40	0.00004	29.4	-1.0	1.0	
	DWB074A	22.47599	22.47605	22.47608		22.47605	-60	-30			30	-60	0.00003	28.8	-1.6	0.8	
										0							
90C (1)	DWA006A	25.28192	25.31312	25.28191	25.28195	25.28192	-31200	31210	-40	30	-10	0	0.00003	29.7	0.0	0.8	
	DWA007A*	23.02853	23.06052		23.02869	23.02866	-31990			30		-130	0.00003	29.2	-3.4	0.8	
	DWA074A	25.94187	25.96879	25.94198	25.94198	25.94193	-26920	26810	0	50	50	-60	0.00003	29.6	-1.6	0.8	
	DWB054A	21.26166	21.29269	21.26217	21.26218	21.26217	-31030	30520	-10	10	0	-510	0.00003	28.5	-13.7	0.8	
										0							
90C (2)	ARC22-51-1	26.25161	26.25152	26.25155		26.25153	90	-30			20	80	0.00003	28.4	2.2	0.8	
	DWA071A	21.86178	21.86184	21.86184		21.86182	-60	0			20	-40	0.00003	28.9	-1.1	0.8	
	DWA101A	25.67270	25.67285	25.67282		25.67281	-150	30			10	-110	0.00003	29.6	-2.9	0.8	

SAW Baths		Weight (g)					Weight Change (µg)					Overall	Overall	S.A. (cm ²)	Corrosion	Uncertainty
Bath T(°C)	Sample	Initial	As removed	1st clean	2nd clean	3rd clean	As removed	Cycle 1	Cycle 2	Cycle 3	Cy1-Cy3	Change (µg)	Uncertainty		Rate (nm/yr)	nm/yr
Ambient	DWA087A	21.87407	21.87400	21.87401		21.87400	70	-10			10	70	0.00003	29.0	2	0.8
	DWA108A	12.06641	12.06641	12.06639	12.06641	12.06641	0	20	-20	0	-20	0	0.00003	26.9	0	0.9
	DWB007A	23.06885	23.06882	23.06880	23.06880	23.06883	30	20	0	-30	-30	20	0.00003	28.8	1	0.8
	DWB008A	16.48133	16.48132	16.48132	16.48133	16.48132	10	0	-10	10	0	10	0.00003	27.7	0	0.8
	DWB017A	11.99601	11.99595	11.99594	11.99600	11.99598	60	10	-60	20	-40	30	0.00003	27.0	1	0.9
	DWB018A	17.91228	17.91224	17.91224		17.91223	40	0			10	50	0.00003	28.0	1	0.8
	DWB033A	18.16247	18.16242	18.16241	18.16243	18.16242	50	10	-20	10	-10	50	0.00003	28.0	1	0.8
60C (1)	ARC22-57-2	26.66349	26.66145	26.66144		26.66145	2040	10			-10	2040	0.00003	28.9	54	0.8
	DWA054A	22.83988	22.83828	22.83826		22.83827	1600	20			-10	1610	0.00003	29.0	43	0.8
	DWB009A	20.48957	20.48787	20.48789		20.48787	1700	-20			20	1700	0.00003	28.2	46	0.8
60C (2)	DWA127A	23.07328	23.07146	23.07148		23.07150	1820	-20			-20	1780	0.00003	29.0	47	0.8
	DWA128A	22.88230	22.88047	22.88049		22.88050	1830	-20			-10	1800	0.00003	29.0	48	0.8
	DWB072A	21.75878	21.75704	21.75707		21.75707	1740	-30			0	1710	0.00003	28.6	46	0.8
	DWB073A	22.12397	22.12224	22.12223		22.12223	1730	10			0	1740	0.00003	28.7	47	0.8
90C (1)	DCA314-1	28.98013	28.96163	28.96165		28.96164	18500	-20			10	18490	0.00003	29.1	487	0.8
	DWB101A	21.97219	21.95485	21.95486		21.95486	17340	-10			0	17330	0.00003	28.7	463	0.8
	DWB102A	21.74952	21.73244	21.73244	21.73246	21.73244	17080	0	-20	20	0	17080	0.00003	28.5	460	0.8
90C (2)	DCA307-2	28.80487	28.78644	28.78643		28.78644	18430	10			-10	18430	0.00004	29.3	483	1.0
	DWA124A	22.18601	22.16854	22.16852		22.16851	17470	20			10	17500	0.00004	29.0	463	1.1
	DWA125A	23.22613	23.20745	23.20744		23.20746	18680	10			-20	18670	0.00003	29.1	492	0.8
	DWB153A	22.71836	22.70068	22.70069	22.70071	22.70072	17680	-10	-20	-10	-30	17640	0.00003	28.7	472	0.8

24 Month Data

NaCl Baths		Weight (g)					Weight Change (µg)			Overall Change (µg)	Overall Uncertainty	S.A. (cm ²)	Corrosion Rate (nm/yr)	Uncertainty nm/yr	
Bath T(°C)	Sample	Initial	As removed	1st clean	2nd clean	3rd clean	As removed	Cycle 1	Cycle 2						Cycle 3
Ambient	ARC22-53-1	25.76987	25.76982	25.76982	25.76985	25.76982	50	-10	-30	30	50	0.00003	28.4	1.0	0.6
	ARC22-58-2	26.36541	26.36544	26.36545	26.36546	26.36545	-20	-10	-10	10	-40	0.00003	27.6	-0.8	0.6
	ARC22-59-2	27.80842	27.80842	27.80844	27.80845	27.80844	0	-10	-10	10	-20	0.00003	29.1	-0.4	0.6
	DCA302-2	30.50303	30.50300	30.50305	30.50301	30.50302	20	-50	40	-10	10	0.00003	29.9	0.2	0.6
	DCA309-1	29.99820	29.99820	29.99825	29.99821	29.99822	0	-50	30	-10	-30	0.00003	29.5	-0.6	0.6
	DCA310-1	25.98230	25.98228	25.98231	25.98234	25.98231	20	-30	-30	40	-10	0.00003	28.6	-0.2	0.6
	DWB141A	18.19613	18.19614	18.19616	18.19617	18.19616	0	-30	-10	10	-30	0.00003	28.2	-0.6	0.6
60C (1)	DCA303-2	30.17889	30.17877	30.17880	30.17885	30.17883	120	-30	-40	20	60	0.00003	29.4	1.2	0.6
	DCA304-2	29.67437	29.67425	29.67431	29.67431	29.67431	110	-50	0	0	60	0.00003	29.6	1.2	0.6
	DWB002A	25.45128	25.45123	25.45123	25.45126	25.45128	50	0	-30	-20	0	0.00003	29.3	0.0	0.6
60C (2)	ARC22-47-1	26.56849	26.56841	26.56844	26.56846	26.56842	90	-30	-30	40	70	0.00003	28.4	1.4	0.6
	ARC22-48-1	25.81430	25.81436	25.81420	25.81420	25.81419	-60	160	0	10	110	0.00003	28.1	2.3	0.6
	ARC22-60-1	25.99621	25.99615	25.99621	25.99620	25.99619	60	-60	10	10	20	0.00003	28.2	0.4	0.6
	ARC22-60-2	26.34534	26.34527	26.34527	26.34531	26.34529	70	0	-40	20	40	0.00003	28.4	0.8	0.6
90C (1)	ARC22-47-2	27.25570	27.25563	27.25562	27.25562	27.25558	70	10	0	40	120	0.00003	29.1	2.4	0.6
	DCA305-1	29.61313	29.61312	29.61311	29.61310	29.61308	10	10	0	20	50	0.00003	29.6	1.0	0.6
	DCA306-1	28.94329	28.94326	28.94325	28.94325	28.94322	30	10	10	30	70	0.00003	29.0	1.4	0.6
90C (2)	ARC22-55-1	26.63050	26.63047	26.63045	26.63044	26.63042	30	30	10	20	80	0.00003	28.3	1.6	0.6
	ARC22-56-1	25.10718	25.10715	25.10712	25.10708	25.10707	30	30	40	10	110	0.00003	28.1	2.3	0.6
	DWA010A	21.84352	21.84360	21.84354	21.84352	21.84353	-80	60	20	-10	-10	0.00003	28.5	-0.2	0.6
	DWA011A	21.79339	21.79346	21.79341	21.79339	21.79338	-70	50	20	10	10	0.00003	28.8	0.2	0.6
SCW Baths		Weight (g)					Weight Change (µg)			Overall Change (µg)	Overall Uncertainty	S.A. (cm ²)	Corrosion Rate (nm/yr)	Uncertainty nm/yr	
Bath T(°C)	Sample	Initial	As removed	1st clean	2nd clean	3rd clean	As removed	Cycle 1	Cycle 2						Cycle 3
Ambient	ARC22-49-2	25.89923	25.89932	25.89924	25.89923	25.89923	-90	80	0	0	0	0.00003	28.1	0.0	0.6
	ARC22-53-2	26.06168	26.06171	26.06163	26.06163	26.06165	-30	90	0	-10	40	0.00003	27.5	0.8	0.6
	DCA307-1	28.54091	28.54096	28.54086	28.54087	28.54090	-50	100	-20	-20	10	0.00003	29.0	0.2	0.6
	DCA311-2	28.46349	28.46353	28.46344	28.46347	28.46347	-40	90	-30	0	30	0.00003	30.1	0.6	0.6
	DWA141A	24.40225	24.40232	24.40222	24.40223	24.40224	-70	100	-10	0	10	0.00003	29.2	0.2	0.6
	DWA151A	24.90171	24.90190	24.90168	24.90172	24.90170	-190	230	-50	20	10	0.00003	28.2	0.2	0.6
	DWB032A	22.66495	22.66500	22.66488	22.66491	22.66493	-50	120	-30	-30	20	0.00003	28.0	0.4	0.6
60C (1)	DWA015A	17.77558	17.77563	17.77558	17.77559	17.77560	-50	50	-10	0	-20	0.00003	29.6	-0.4	0.6
	DWA114A	23.76673	23.76680	23.76675	23.76677	23.76677	-80	60	-20	0	-50	0.00003	29.5	-1.0	0.6
	DWB077A	11.84111	11.84113	11.84112	11.84113	11.84113	-20	0	0	0	-20	0.00003	29.1	-0.4	0.6
60C (2)	DWA017A	17.67794	17.67800	17.67802	17.67801	17.67801	-60	-30	10	0	-70	0.00003	28.4	-1.4	0.6
	DWA072A	26.37575	26.37592	26.37591	26.37589	26.37587	-170	10	10	30	-120	0.00003	27.6	-2.5	0.6
	DWB082A	23.82290	23.82291	23.82290	23.82291	23.82292	-10	10	-20	0	-20	0.00003	28.1	-0.4	0.6
	DWB083A	21.34847	21.34855	21.34854	21.34851	21.34856	-80	10	20	-40	-90	0.00003	27.9	-1.9	0.6
90C (1)	ARC22-43-2	27.33695	27.40355				-66600						28.9		
	DWA012A	23.08592	23.14488	23.08571			-58950	59160					29.6		
	DWA014A	17.62983	17.68489	17.62973			-55050	55150					29.0		
90C (2)	DCA295-1	28.93961	28.93960	28.93942			10	180					28.1		
	DWA075A	26.13922	26.13944	26.13926			-210	180					27.7		
	DWA076A	25.96944	25.96961	25.96945			-170	160					28.5		
	DWB043A	21.67889	21.68434	21.67851			-5450	5830					28.7		

SAW Baths		Weight (g)					Weight Change (µg)				Overall	Overall	S.A. (cm ²)	Corrosion	Uncertainty
Bath T(°C)	Sample	Initial	As removed	1st clean	2nd clean	3rd clean	As removed	Cycle 1	Cycle 2	Cycle 3	Change (µg)	Uncertainty		Rate (nm/yr)	nm/yr
Ambient	DCA308-2	29.86969	29.86963	29.86962	29.86958	29.86960	60	10	30	-20	90	0.00003	29.3	2	0.6
	DWA041A	25.72248	25.72244	25.72240	25.72241	25.72243	40	40	0	-20	50	0.00003	29.5	1	0.6
	DWA042A	24.11429	24.11429	24.11428	24.11424	24.11427	10	0	40	-20	20	0.00003	29.2	0	0.6
	DWA044A	21.70657	21.70652	21.70650	21.70649	21.70650	50	10	10	-10	70	0.00003	28.8	1	0.6
	DWA057A	22.99906	22.99890	22.99888	22.99883	22.99887	170	20	50	-40	200	0.00003	29.1	4	0.6
	DWA058A	22.75584	22.75570	22.75568	22.75565	22.75568	140	20	30	-30	160	0.00003	29.1	3	0.6
	DWB078A	22.74834	22.74834	22.74833	22.74830	22.74832	10	10	30	-20	20	0.00003	28.7	0	0.6
60C (1)	DWA043A	26.20098	26.19860	26.19861	26.19859	26.19862	2380	-10	20	-30	2360	0.00003	29.6	46	0.6
	DWA173A	25.63288	25.63071	25.63070	25.63071	25.63071	2170	10	-10	0	2170	0.00003	29.2	43	0.6
	DWB031A	18.88805	18.88578	18.88580	18.88580	18.88580	2270	-20	0	0	2260	0.00003	28.2	46	0.6
60C (2)	DWA045A	16.56000	16.55769	16.55768	16.55767	16.55767	2310	10	10	10	2330	0.00003	27.9	48	0.6
	DWA046A	23.89473	23.89240	23.89239	23.89238	23.89237	2330	10	0	20	2360	0.00003	29.3	46	0.6
	DWB164A	18.62017	18.61798	18.61795	18.61796	18.61795	2190	30	-10	10	2210	0.00003	27.8	46	0.6
	DWB166A	21.28435	21.28213	21.28213	21.28211	21.28213	2230	0	20	-30	2220	0.00003	28.3	45	0.6
90C (1)	DWA084A	21.79453	21.77122	21.77124	21.77123	21.77125	23310	-20	10	-30	23270	0.00003	28.8	465	0.6
	DWA085A	21.94355	21.92069	21.92070	21.92070	21.92067	22860	-10	0	30	22890	0.00003	28.8	457	0.6
	DWA121A	23.05811	23.03546	23.03547	23.03541	23.03548	22650	0	50	-70	22630	0.00003	29.0	449	0.6
90C (2)	ARC22-56-2	26.40684	26.38419	26.38418	26.38414	26.38417	22650	20	30	-20	22670	0.00003	29.0	450	0.6
	DWA018A	22.75573	22.73170	22.73172	22.73167	22.73169	24030	-20	50	-20	24040	0.00003	29.1	475	0.6
	DWA031A	25.75402	25.73081	25.73082	25.73080	25.73081	23210	-10	20	-10	23210	0.00003	29.5	453	0.6
	DWB142A	18.25600	18.23419	18.23419	18.23418	18.23420	21810	0	10	-20	21800	0.00003	27.8	451	0.6